THE PENNSYLVANIA
STATE UNIVERSITY

IONOSPHERIC RESEARCH

Scientific Report No. 353

TIME OF FLIGHT MASS SPECTROMETRY FOR IONOSPHERIC MEASUREMENTS: THEORY AND EXPERIMENTS

by
M. F. Zabielski

April 10, 1970

IONOSPHERE RESEARCH LABORATORY

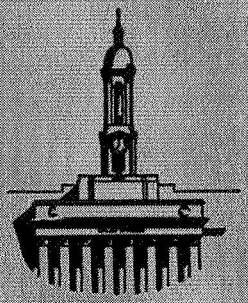

University Park, Pennsylvania NASA Grant NGR 39-009-129

Ionospheric Research

NASA Grant NGR 39-009-129

Scientific Report

on

"Time of Flight Mass Spectrometry for Ionospheric Measurements: Theory and Experiment"

by

M. F. Zabielski

April 10, 1970

Scientific Report No. 353

Submitted by: B. R. F. Kendall (mw)

B. R. F. Kendall, Project Supervisor

Approved by: A. H. Waynick

A. H. Waynick, Director
Ionosphere Research Laboratory

Ionosphere Research Laboratory

The Pennsylvania State University

TABLE OF CONTENTS

ABSTRACT

Theoretical analyses are made of cylindrical, planar, and spherical time-of-flight mass spectrometers with two accelerating regions. The results of these analyses are compared and indicate that for the flight paths considered, the space focusing of the spherical device is superior to that of the other two geometries and the space focusing of the cylindrical geometry is superior to that of the planar geometry.

The results of an experimental investigation of a small cylindrical wedge time-of-flight mass spectrometer are presented. These results suggest that this instrument is suitable for making measurements at least down to the middle of the D-region of the ionosphere. The primary reasons for this suitability are high sensitivity and the ability to function at the high ambient pressures encountered in the D-region.

The mechanical and electronic design of an experiment package suitable for flight on a small sounding rocket is described. The mechanical design is presented within the requirements imposed by the small rocket. The electronic design is presented in block function form. Suggestions for future experiment packages are also given.

I. INTRODUCTION

General

The ionosphere has provided the impetus for a large amount of interaction among physical scientists, engineers and mathematicians. Crudely, it can be defined as that part of the earth's ionized atmosphere which is located approximately between 50 and 1000 kilometers in altitude. At least two things have stimulated this interaction between such a broad spectrum of investigators. The first has been the myriad of physical processes which constitute the "weather" in this region with its influence on communications. The second has been the fact that this "weather" in the ionosphere is most directly influenced by the sun and thus provides information about the sun.

Since Chapman (1931) developed the first good quantitative description of an ionospheric layer, people have endeavored to construct models which incorporate these layers. Actually, the word "layer" is slightly misleading in that in situ experiments do not show well defined layers but regions of large gradients in electron concentrations. The present classification of regions in the ionosphere is: the D-region which is between 60 kilometers and 90 kilometers; the E-region which is between 90 kilometers to 140 kilometers; the F_1 region which is between 140 kilometers and 200 kilometers; and finally the F_2 region which lies between 200 kilometers and 300 kilometers. Above 300 kilometers is generally known as the 'topside.'

In order to construct a model, one needs several inputs: primarily, the temperature of the neutral and ionic gases and of the electrons, the pressure, the chemical composition and kinetic rates of both neutrals and ions, the wavelengths and intensities of solar radiation. It is the purpose of this work to discuss a means of determining one of these inputs; namely, the composition of the ionized gases and their relative concentrations. The means that will be considered is mass spectrometry.

Mass Spectrometry in the Upper Atmosphere

The application of mass spectrometric techniques to the upper atmosphere is not new. The pioneering work in this area was conducted at the Naval Research Laboratory by C.Y. Johnson and E.B. Meadows (1955), C.Y. Johnson and J.P. Heppner (1955), and J.W. Townsend (1952). The original flights surveyed the D, E, and lower F regions. The results of most of these flights are in doubt but the feasibility of mass spectrometry in the ionosphere was established. The instrument that was employed was a Bennett RF spectrometer with a resolving power of about 25.

A host of other experimenters have entered the field. Some of the more prominent people have been: Boyd (1955, 1959, 1960), Sayers (1959), Nier and Hedin (1967), Hoffman (1967, 1969), Istomin (1961, 1963), Holmes (1959), Pokhunkov (1960, 1963), Schaeffer (1964), and von Zahn (1967). These people have primarily concentrated their work to the E and F regions. These regions are areas of low pressure and are ideally suited for measurements by

mass spectrometers. However, the D-region is a relatively high pressure region where the local mean free paths are comparable or smaller than the dimensions of most mass spectrometers. The only experimenter who has been making measurements in this region for a prolonged period of time is R.S. Narcisi (1965, 1966, 1967). Other scientists who have entered into this work just recently have been R. Goldberg and S. Bauer (1968), J. Zahringer (1969), and T.M. Donahue (1968). The type of mass spectrometer that has been used by all these investigators has been the quadrupole which was first constructed by W. Paul and M. Raether (1955). To circumvent the problems associated with the high pressure, these investigators have used cryopumps and ion pumps which maintain the pressure in the spectrometer region well below that of the ambient. Ions or neutral gases have been introduced into the spectrometer region through an orifice which is typically four thousandths of an inch in diameter. The bulk of these D-region measurements have been positive ion measurements. R.S. Narcisi, however, has flown several negative ion mass spectrometers (1968, 1969).

Time-of-Flight Mass Spectrometry

The instruments considered in this presentation are not of a quadrupole design but of a time-of-flight design. The time-of-flight principle was developed independently by Stephens (1946) and Cameron and Eggers (1948). Several people such as Keller (1949), Takekoshi *et al* (1951), Glenn (1951, 1952), Wolf and Stephens (1953), and Katzenstein and Friedland (1955) participated in the investigation of this technique.

Time-of-flight spectrometers can be classified as either "constant energy" or "constant momentum" devices. In a "constant energy" device, ions of different masses and the same charge are given essentially the same energy. The lighter mass ions will arrive at a detector sooner than the heavier mass ions. In the "constant momentum" device, ions are given uniform momentum and again the lighter ions will be detected before the heavier ion. In both cases, a relationship between the ionic mass and the time it takes to travel a given distance can be determined. In 1955 Wiley and McLaren introduced a "constant energy" instrument with a resolving power of more than double that of the instruments developed to that time. [Its superior performance was due to its ion source design which had a double accelerating region.] This instrument, as well as the other instruments referenced, incorporated planar grid assemblied.

MacKenzie (1964) designed a time-of-flight instrument of a cylindrical geometry for use in making measurements in the E-region of the ionosphere. This instrument had a flight path of approximately 12 cm. It did not incorporate the features of the Wiley and McLaren instrument and was a low resolving power device, typically 3 as defined as width at half-height and under the constraints of the ion source used in the laboratory. This instrument was successfully flown and it had sufficient resolving power to indicate the presence of NO^+ and O_2^+.

In 1967, Diem (1967) reported preliminary results obtained with a time-of-flight mass spectrometer incorporating a double accelerating region similar to that Wiley and McLaren (1955) and cylindrical geometry similar to that of MacKenzie (1964). This author participated in this preliminary work and extended it with a presentation by Zabielski, Diem, and Kendall (1968).

Statement of Problem

The principal objectives of this work are threefold. The first is a theoretical investigation and comparison of time-of-flight mass spectrometers of cylindrical, planar, and spherical geometries. The second is the experimental study of a cylindrical wedge time-of-flight mass spectrometer and of its suitability for making measurements in the D-region. Finally, the third is the development of an experiment package based on the wedge spectrometer for a flight on a small sounding rocket.

II. THEORY

Cylindrical Two Field Spectrometer

Figure 1 shows a cross-section of a cylindrical spectrometer consisting of three cylindrical grids and an axial cylindrical collector. We shall assume that positive ions enter or are formed in region 1. The outermost grid is periodically pulsed upward in potential from its normal potential V_2 to a potential $V_2 + P(t)$, thus producing an inwards radial acceleration of all ions in region 1. The pulse P(t) is maintained until all ions have moved out of region 1. The ions starting from larger radii acquire more energy than those originating from smaller radii. The ions are further accelerated by the potential difference existing between grids two and three and enter region 3 which is a field free area. In this third region the ions drift at constant velocity until they reach the collector which has a radius r_c.

We now proceed to determine the relationship between mass and time as a function of the starting radii of the ions, of the radii of the electrodes and collector, of the potentials that exist at the electrodes, and of the ionic initial energies. Since regions 1 and 2 are geometrically and electrically similar, we shall derive a set of generalized equations which describe the field and the ionic motion in a cylindrically symmetric slab. We shall assume that the charge density in this slab is negligible so that Laplace's equation holds. We shall also assume that the end

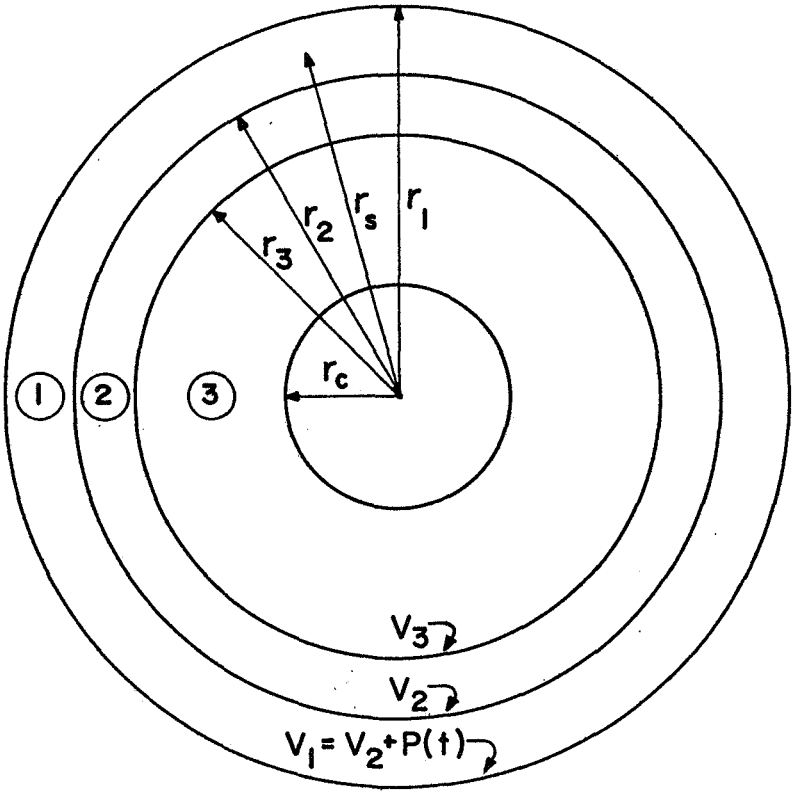

FIGURE 1. CROSS SECTION OF CYLINDRICAL TIME-OF-FLIGHT MASS SPECTROMETER WITH TWO ACCELERATING REGIONS

effects of the cylinder are small and can be neglected; thus, we write only the radial term of Laplace's equation

$$\nabla^2 V = 0 \tag{1}$$

$$\frac{1}{r} \frac{d}{dr} \left(r \frac{dV}{dr} \right) = 0 \ . \tag{2}$$

The first integration yields

$$r \frac{dV}{dr} = C_1 \ . \tag{3}$$

The second integration yields

$$V(r) = C_1 \ln r + C_2 \ . \tag{4}$$

Now, in a generalized scheme let $r_i > r_j$ and $V_i > V_j$, the potentials on the electrodes at r_i and r_j respectively. To solve for the constants C_1 and C_2, we apply the boundary conditions, thus

$$V_i = C_1 \ln r_i + C_2 \tag{5}$$

$$V_j = C_1 \ln r_j + C_2 \ . \tag{6}$$

Subtracting equation (6) from equation (5), we get

$$V_i - V_j = C_1 \ (\ell n \ r_i - \ell n \ r_j), \tag{7}$$

therefore

$$C_1 = \frac{V_i - V_j}{\ell n \ (r_i/r_j)} \quad . \tag{8}$$

To solve for C_2, we place the value of C_1 into equation (5)

$$V_i = \frac{(V_i - V_j)}{\ell n \ (r_i/r_j)} \quad \ell n \ r_i + C_2 \ , \tag{9}$$

which yields

$$C_2 = V_i - \frac{(V_i - V_j) \ \ell n \ r_i}{\ell n \ (r_i/r_j)} \tag{10}$$

Thus, we have the potential V(r)

$$V(r) = \frac{(V_i - V_j) \ \ell n \ (r/r_i)}{\ell n \ (r_i/r_j)} + V_i \tag{11}$$

which is the potential distribution between r_i and r_j.

Next we move on to the equation of motion for an ion present in such a cylindrical slab which is simply

$$m \frac{d^2\vec{r}}{dt^2} = q \vec{E}(r) \tag{12}$$

where m is the mass of the particle, q is its charge, and E(r) is the field. E(r) is determined by the negative of the gradient of V(r) which is given by equation (11), thus

$$\vec{E}(r) = - \frac{dV}{dr} \hat{a}_r \tag{13}$$

$$\vec{E}(r) = - \frac{(V_i - V_j)}{\ell n\ (r_i/r_j)} \frac{1}{r} \hat{a}_r \tag{14}$$

where $\hat{a}_r$ is a unit vector in the outward radial direction. Consequently, we have the second order ordinary differential equation

$$\frac{d^2r}{dt^2} = - \frac{q}{m} \frac{(V_i - V_j)}{\ell n\ (r_i/r_j)} \frac{1}{r} . \tag{15}$$

For manipulative purposes, let $K_{ij} = (V_i - V_j)/\ell n\ (r_i/r_j)$ then

$$\frac{d^2r}{dt^2} = -\frac{q}{m}\frac{K_{ij}}{r} \quad . \tag{16}$$

Rewriting and multiplying by dr yields

$$\frac{dr}{dt}\ d\left(\frac{dr}{dt}\right) = -\frac{q\ K_{ij}}{m}\ \frac{dr}{r} \tag{17}$$

which upon integration is

$$\frac{1}{2}\left(\frac{dr}{dt}\right)^2 = -\frac{qK_{ij}}{m}\ \ell n\ r + C_3 \quad . \tag{18}$$

Next we employ the initial conditions which are that at $t = 0$, $r = r_k$ where the subscript $\underline{k}$ denotes the starting radius, and $(dr/dt) = \pm v_0$ where v_0 is the initial velocity for which we allow the possibility of being directed both inwardly or outwardly, therefore

$$C_3 = \frac{q}{m}\ K_{ij}\ \ell n\ r_k + \frac{1}{2}\ (\pm v_0)^2 \tag{19}$$

which makes equation (18)

$$\left(\frac{dr}{dt}\right)^2 = \frac{2q}{m} K_{ij} \ln (r_k/r) + v_0^2 \quad . \tag{20}$$

In order to perform the second integration, we take the square root, thus

$$\pm \frac{dr}{dt} = \sqrt{\frac{2q}{m} K_{ij} \ln (r_k/r) + v_0^2} \tag{21}$$

Rewriting gives

$$\pm dt = \frac{dr}{\sqrt{\frac{2q}{m} K_{ij} \ln (r_k/r) + v_0^2}} . \tag{22}$$

Let $x = \ln(r_k/r)$, then $dr = - r_k e^{-x} dx$, which upon substitution into equation (22) yields

$$dt = \frac{\pm r_k e^{-x} dx}{\sqrt{\frac{2q}{m} K_{ij} x + v_0^2}} \tag{23}$$

Let $y = \left(\frac{2q\ K_{ij}}{m}\right) x + v_0^2$, then $dy = \left(\frac{2q\ K_{ij}}{m}\right) dx$, which upon substitution into equation (23) yields

$$dt = \pm \frac{r_k m\, e^{-\left[\frac{m}{2qK_{ij}} (y - v_0^2)\right]} dy}{2q\ K_{ij}\ \sqrt{y}} . \tag{24}$$

Rewriting gives

$$dt = \pm \frac{r_k m\, e^{\frac{m v_0^2}{2q\ K_{ij}}}}{2q\ K_{ij}} \frac{e^{-\frac{my}{2q\ K_{ij}}}}{y^{1/2}} dy . \tag{25}$$

Next, let $z = my/2q\ K_{ij}$, then using $dy = 2q\ K_{ij}\ dz/m$, yields

$$dt = \pm \frac{r_k e^{\frac{m v_0^2}{2q\ K_{ij}}}}{(2q\ K_{ij}/m)^{1/2}} \frac{e^{-z}}{z^{1/2}} dz . \tag{26}*$$

*If $z = p^2$ is chosen, $dt = \pm \frac{2r_k e^{\frac{m v_0^2}{2qK_{ij}}}}{(2qK_{ij}/m)^{1/2}} e^{-p^2} dp$ which is the form of an error function.

Expanding e^{-z} in a Maclaurin series produces

$$dt = \pm \frac{r_k e^{\frac{m v_0^2}{2q K_{ij}}}}{(2q K_{ij}/m)^{1/2}} \sum_{n=0}^{\infty} \frac{(-1)^n z^n}{n! z^{1/2}} dz , \tag{27}$$

so that

$$dt = \pm \frac{r_k e^{\frac{m v_0^2}{2q K_{ij}}}}{(2q K_{ij}/m)^{1/2}} \sum_{n=0}^{\infty} \frac{(-1)^n z^{(n-1/2)}}{n!} dz . \tag{28}$$

Integrating term by term yields

$$t = \pm \frac{r_k e^{\frac{m v_0^2}{2q K_{ij}}}}{(2q K_{ij}/m)^{1/2}} \sum_{n=0}^{\infty} \frac{(-1)^n z^{(n+1/2)}}{n!(n + 1/2)} + C_4 . \tag{29}$$

Transforming back into r-space, one obtains

$$t = \pm \frac{r_k^e}{\left(\frac{m v_0^2}{2q K_{ij}}\right)} \frac{\left(2q K_{ij}/m\right)^{1/2}}{} \sum_{n=0}^{\infty} \frac{(-1)^n}{n!\,(n + 1/2)} \cdot$$

$$\left(\ln(r_k/r) + \frac{m v_0^2}{2q K_{ij}} \right)^{n+1/2} + C_4 \cdot \tag{30}$$

Applying the initial conditions $t = 0$, $r = r_k$ and choosing the appropriate signs necessary to have a positive value for the time yields

$$t = \frac{r_k^e}{\left(\frac{m v_0^2}{2q K_{ij}}\right)} \frac{\left(2q K_{ij}/m\right)^{1/2}}{} \sum_{n=0}^{\infty} \frac{(-1)^n}{n!(n + 1/2)} \cdot$$

$$\left\{ \left(\ln (r_k/r) + \frac{m v_0^2}{2q K_{ij}} \right)^{n+1/2} - \left(\frac{m v_0^2}{2q K_{ij}} \right)^{n+1/2} \right\} . \tag{31}$$

In order to account for the case where the ion has an outward radial velocity, the turn around time must be included. By employing equation (11), the radius at which the ion is stopped is

$$r^{+} = r_i e^{\left(V_k - V_i + \frac{1}{2}\frac{m v_0^2}{2q K_{ij}}\right) \ln (r_i/r_j)/(V_i/V_j)} \tag{32}$$

where V_k is the potential at the starting position of the ion. Thus, for an ion with an initial velocity that is directed in the positive radial direction, the flight time is

$$t = \frac{r_k e^{\frac{m v_0^2}{2q K_{ij}}}}{(2q K_{ij}/m)^{1/2}} \sum_{n=0}^{\infty} \frac{(-1)^n}{n!(n+1/2)} \cdot$$

$$\left\{ \left(\ln (r_k/r) + \frac{m v_0^2}{2q K_{ij}} \right)^{n+1/2} - \left(\frac{m v_0^2}{2q K_{ij}} \right)^{n+1/2} \right\}$$

$$- \frac{2r_k e^{\frac{m v_0^2}{2q K_{ij}}}}{(2q K_{ij}/m)^{1/2}} \sum_{n=0}^{\infty} \frac{(-1)^n}{n!(n + 1/2)} \cdot$$

$$\left(\ell n \, (r_k/r^+) + \frac{m v_0^2}{2q K_{ij}} \right)^{n+1/2} - \left(\frac{m v_0^2}{2q K_{ij}} \right)^{n+1/2} \cdot \qquad (33)$$

The second term in equation (33) is preceded by a minus sign because $r^+ > r_k$. Also a factor of 2 multiplies this term because the turn around time is twice the stopping time. The time spent in a given region terminating at r_j can then be written

$$T_i^{(P)} = \frac{r_k e^{\frac{m v_0^2}{2q K_{ij}}}}{(2q K_{ij}/m)^{1/2}} \sum_{n=0}^{\infty} \frac{(-1)^n}{n!(n + 1/2)} \left\{ \left(\ell n \, (r_k/r_j) + \frac{m v_0^2}{2q K_{ij}} \right)^{n+1/2} \right.$$

$$\left. - \left(\frac{m v_0^2}{2q K_{ij}} \right)^{n+1/2} \right\} - \frac{2r_k e^{\frac{m v_0^2}{2q K_{ij}}}}{(2q K_{ij}/m)^{1/2}} \sum_{n=0}^{\infty} \frac{(-1)^n}{n!(n + 1/2)} \cdot$$

$$\left\{ \left(\ell n \ (r_k/r^+) + \frac{m \ v_0^{\ 2}}{2q \ K_{ij}} \right)^{n+1/2} - \left(\frac{m \ v_0^{\ 2}}{2q \ K_{ij}} \right)^{n+1/2} \right\} \tag{34a}$$

$$T_i^{(N)} = \frac{r_k \ e^{\frac{mv_0^{\ 2}}{2qK_{ij}}}}{(2qK_{ij}/m)^{1/2}} \sum_{n=0}^{\infty} \frac{(-1)^n}{n!(n+1/2)}$$

$$\left\{ \left(\ell n(r_k/r_j) + \frac{mv_0^{\ 2}}{2qK_{ij}} \right)^{n+1/2} - \left(\frac{mv_0^{\ 2}}{2qK_{ij}} \right)^{n+1/2} \right\} \tag{34b}$$

where the superscripts P and N refer to initial positive and negative radial velocities respectively and the subscript i refers to the region under consideration.

We are now in a position to write the time spent in regions 1 and 2 by employing equation (34). For region 1, $r_i = r_1$, $r_j = r_2$, $r_k = r_s$ where $r_1 > r_s > r_2$, $K_{ij} = K_{12} = (V_1 - V_2)/\ell n(r_1/r_2)$ and $v_0 = v_s$ which is the velocity characteristic of the source producing the ions and/or of the method of introducing the ions into this region. Hence, we may write

For region 2, $r_i = r_2$, $r_j = r_3$, $r_k = r_2$, $K_{ij} = K_{23} = \dfrac{(V_2 - V_3)}{\ell n(r_2/r_3)}$.

But, before we proceed to apply equation (34a,b), we must determine v_0 for this region. We know that the energy of the ion as it enters this region is

$$\frac{1}{2} m v_0^2 = \frac{1}{2} m v_s^2 + q (V_s - V_2). \tag{36}$$

In order to determine V_s which is the potential at r_s, we use equation (11) which gives

$$V_s = \frac{(V_1 - V_2) \ell n (r_s/r_1)}{\ell n (r_1/r_2)} + V_1 \tag{37}$$

Rewriting equation (36) for v_0^2 yields

$$v_0^2 = v_s^2 + \frac{2q}{m} (V_s - V_2) \tag{38}$$

which with the substitution of equation (37) becomes

$$v_0^2 = v_s^2 + \frac{2q}{m} \frac{(V_1 - V_2) \ell n (r_s/r_2)}{\ell n (r_1/r_2)} = \beta^2 \tag{39}$$

where β is used to denote the fact that the second region is being considered. In the derivation of equation (34), it was useful to allow radially inward and outward initial velocities. However, in region 2, ions can only have an inward velocity, so only equation (34b) need be considered. Thus, the time spent in region 2 is

$$T_2 = \frac{r_2 e^{\frac{m\beta^2}{2qK_{23}}}}{(2qK_{23}/m)^{1/2}} \sum_{n=0}^{\infty} \frac{(-1)^n}{n!(n+1/2)} \left\{ \left(\ell n(r_2/r_3) + \frac{m\beta^2}{2qK_{23}} \right)^{n+1/2} - \left(\frac{m\beta^2}{2qK_{23}} \right)^{n+1/2} \right\} \tag{40}$$

We have now surmounted the major obstacles in computing the total time of flight of an ion. The third region is field free, so the ions simply coast; thus, the time spent in this region is merely the radial distance of the region divided by the velocity of the ion at its entrance into the region. This yields

$$T_3 = \frac{r_3 - r_c}{\left[v_s^2 + \frac{2q}{m}(V_s - V_3)\right]^{1/2}} \tag{41}$$

where V_s has already been defined by equation (37). For reasons which will become obvious shortly, equation (41) is rewritten

$$T_3 = \frac{r_3 - r_c}{(2q/m)^{1/2}\left[\frac{mv_s^2}{2q} + (V_s - V_3)\right]^{1/2}} \tag{42}$$

The total time of flight for an ion starting at a radius r_s with an initial velocity v_s is the sum of equations (35), (40) and (42) which is

$$T_t^{(P)} = m^{1/2} \left[\frac{r_s e^{\frac{mv_s^2}{2qK_{12}}}}{(2qK_{12})^{1/2}} \sum_{n=0}^{\infty} \frac{(-1)^n}{n!(n+1/2)} \right.$$

$$\left\{ \left(\ell n(r_s/r_2) + \frac{mv_s^2}{2qK_{12}} \right)^{n+1/2} - \left(\frac{mv_s^2}{2qK_{12}} \right)^{n+1/2} \right\} - \frac{2r_s e^{\frac{mv_s^2}{2qK_{12}}}}{(2qK_{12})^{1/2}} \cdot$$

$$\sum_{n=0}^{\infty} \frac{(-1)^n}{n!(n+1/2)} \left\{ \left(\ell n(r_s/r^+) + \frac{mv_s^2}{2qK_{12}} \right)^{n+1/2} - \left(\frac{mv_s^2}{2qK_{12}} \right)^{n+1/2} \right\}$$

$$+ \frac{r_2 e^{\frac{m\beta^2}{2qK_{23}}}}{(2qK_{23})^{1/2}} \sum_{n=0}^{\infty} \frac{(-1)^n}{n!(n+1/2)} \left\{ \left(\ell n(r_2/r_3) + \frac{m\beta^2}{2qK_{23}} \right)^{n+1/2} \right.$$

$$\left. \left. - \left(\frac{m\beta^2}{2qK_{23}} \right)^{+1/2} \right\} + \frac{(r_3 - r_c)}{(2q)^{1/2} \left[\frac{mv_s^2}{2q} + (V_s - V_3) \right]^{1/2}} \right] \qquad (43a)$$

$$T_t(M) = m^{1/2}\left[\frac{r_s e^{\frac{mv_s^2}{2qK_{12}}}}{(2qK_{12})^{1/2}}\sum_{n=0}^{\infty}\frac{(-1)^n}{n!(n+1/2)}\right.$$

$$\left\{\left(\ell n(r_s/r_2) + \frac{mv_s^2}{2qK_{12}}\right)^{n+1/2} - \left(\frac{mv_s^2}{2qK_{12}}\right)^{n+1/2}\right\}$$

$$+ \frac{r_2 e^{\frac{m\beta^2}{2qK_{23}}}}{(2qK_{23})^{1/2}}\sum_{n=0}^{\infty}\frac{(-1)^n}{n!(n+1/2)}$$

$$\left\{\left(\ell n(r_2/r_3) + \frac{m\beta^2}{2qK_{23}}\right)^{n+1/2} - \left(\frac{m\beta^2}{2qK_{23}}\right)^{n+1/2}\right\}$$

$$\left. + \frac{(r_3 - r_c)}{(2q)^{1/2}\left[\frac{mv_s^2}{2q} + (V_s - V_3)\right]^{1/2}}\right] \qquad (43b)$$

where $m^{1/2}$ has been factored out of the denominator of each term.

Recall that the primary purpose of this derivation was to establish the relationship between time and mass, but as is easily seen, the mass factor is apparently liberally distributed among the terms of equation (43a,b), so let us scrutinize these terms. Let us consider those terms which have the general form $mv_0^2/2q\ K_{ij}$. Upon inspection, it is obvious that this is the initial kinetic energy of the ion ($mv_0^2/2$) divided by a term which is only dependent on electrode potentials and radii. In region 1, this initial kinetic energy depends on the method of production of the ion and/or its introduction into this region, so in essence $mv_0^2/2$ can be written U_0 and thus independent of mass as far as the calculation is concerned. In region 2, this initial kinetic energy depends on the energy of creation and/or introduction plus the energy acquired from the field in region 1, so that the initial energy at the entrance of region 2 can be written $U_0 + U_{f1}$ where U_{f1} is the energy acquired from the field in region 1. Similarly, the sum term in the denominator of time equation for region 3 is independent of mass since it is simply the sum of the energies $U_0 + U_{f1} + U_{f2}$ where U_{f2} is the energy acquired from the field of region 2. As a consequence of this analysis, we are left with only a root m dependence; thus it is that equation (43) has the general form

$$T_t = g(r_s, r_1, r_2, r_3, V_1, V_2, V_3, U, q)\sqrt{m} \qquad (44)$$

Thus, we have established the relation between the mass and the flight time of an ion and it conforms to that which was intuitively expected.

Planar Two Field Spectrometer

Before we proceed to investigate equation (43), let us develop the equations of motion for a two field mass spectrometer with planar electrodes. This, as has already been stated, was developed by Wiley and McLaren (1955) and what shall be presented here has been adapted from their presentation. Figure 2 is a side view of the spectrometer. We shall assume again that positive ions are formed in or introduced into region 1. The potential V_1 is equal to $V_2 + P(t)$ where $P(t)$ is a periodic square pulse. The duration of $P(t)$ is such that all ions in region 1 are accelerated into region 2. The ion which travels the greater distance in region 1 will acquire the greater energy. The ions are further accelerated in region 2, which has a constant electric field, and enter region 3 where they drift at constant velocity -- region 3 being field free -- until they reach the collector.

A generalized notation will be employed again. Because of the planar structure, a uniform electric field exists between the electrodes in regions 1 and 2 whose magnitude is given by equation (45)

$$E_i = \frac{V_i - V_j}{s_i} \tag{45}$$

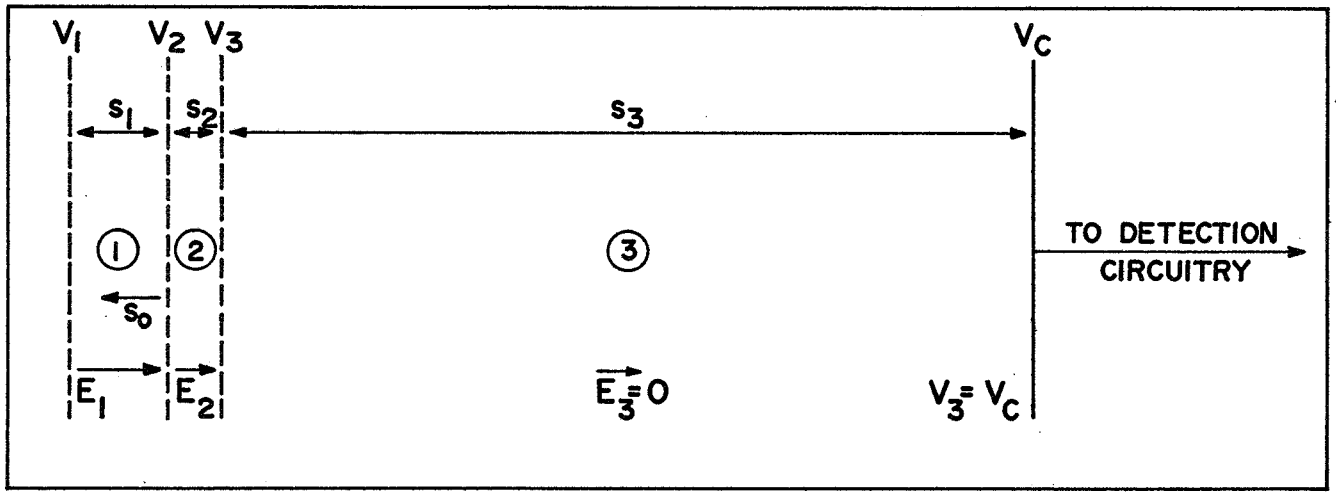

FIGURE 2. SIDE VIEW OF LINEAR TIME-OF-FLIGHT MASS SPECTROMETER OF WILEY AND McLAREN

where s_i is the interelectrode distance. The equation of motion is

$$\frac{md^2x_i}{dt^2} = qE_i \tag{46}$$

where the origin of the i^{th} coordinate system is located at the j^{th} grid and thus all starting positions are negative in this system and the field's directions are positive. We can immediately integrate equation (48) twice yielding

$$x_i = \frac{qE_i t^2}{2m} + C_5 t + C_6 \tag{47}$$

Applying the initial conditions, i.e., at $t = 0$, $x_i = -x_s$ and $dx_i/dt = \pm v_0$, results in $C_5 = \mp v_0$ and $C_6 = -x_s$. Substituting these quantities into equation (47) and rewriting, we get

$$t^2 \mp \frac{2mv_0 t}{qE_i} - \frac{2mx_s}{qE_i} = \frac{2mx_i}{qE_i} \tag{48}$$

To solve for the time spent in the region by the ion, we simply let $x_i = 0$, then

$$T_i^2 \mp \frac{2mv_0 T_i}{qE_i} - \frac{2mx_s}{qE_i} = 0 \tag{49}$$

which upon solving for T_i yields

$$T_i = \sqrt{\frac{m^2 v_0^2}{q^2 E_i^2} + \frac{2m_s}{qE_i}} \pm \frac{mv_0}{qE_i} \quad . \tag{50}$$

If we factor out $(2m)^{1/2}/qE_i$, then equation (50) becomes

$$T_i = \frac{(2m)^{1/2}}{qE_i} \left[\left(qx_s E_i + \frac{mv_0^2}{2} \right)^{1/2} \pm \left(\frac{mv_0^2}{2} \right)^{1/2} \right] \quad . \tag{51}$$

We are now in a position to write the times spent in regions 1 and 2. In region 1, $x_s = s_0$, $E_i = E_1 = (V_1 - V_2)/s_1$, $v_0 = v_s$ which is the velocity characteristic of the source producing the ions and/or the method of introduction of the ions into this region, thus,

$$T_1 = \frac{(2m)^{1/2} s_1}{q(V_1 - V_2)} \left[\sqrt{\frac{qs_0(V_1 - V_2)}{s_1} + \frac{mv_s^2}{2}} \pm \left(\frac{mv_s^2}{2} \right)^{1/2} \right] \tag{52}$$

For region 2, $x_s = s_2$, $E_i = E_2 = (V_2-V_3)/s_2$ and v_0^2 $= v_s^2 + (2q/m)(V_s-V_2)$ where $V_s = (V_1-V_2)s_0/s_1 + V_2$. If we place V_s into the velocity equation, then, for region 2, v_0^2 $= v_s^2 + (2qs_0/m)((V_1-V_2)/s_1) = \gamma^2$. Substituting these quantities into equation (51) yields

$$T_2 = \frac{(2m)^{1/2}s_2}{q(V_2-V_3)} \left[\left(q(V_2-V_3) + \frac{m\gamma^2}{2} \right)^{1/2} - \left(\frac{m\gamma^2}{2} \right)^{1/2} \right] \qquad (53)$$

where, as we had done in the cylindrical case, the plus term in front of $(m\gamma^2/2)^{1/2}$ has been dropped because in region 2 the ions have a velocity component only in the direction of the collector.

In region 3, the ions simply drift, so the time spent in this region is the distance between grid 3 and the collector divided by the velocities which they have upon entry into the region. The initial velocity for region 3 is given by $v_0 = [v_s^2 + (2q/m)(V_s-V_3)]^{1/2}$ where V_s has been defined above, thus

$$T_3 = \frac{(m)^{1/2}s_3}{[mv_s^2 + 2q(V_s-V_3)]^{1/2}} \; . \qquad (54)$$

Consequently, the total time of flight for an ion starting at s_0 is the sum of equations (52), (53) and (54) which is

$$T_t = \sqrt{m}\left[\frac{\sqrt{2\ s_1}}{q(V_1-V_2)}\left\{\left(\frac{qs_0(V_1-V_2)}{s_1}+\frac{mv_s^{\,2}}{2}\right)^{1/2} \pm \left(\frac{mv_s^{\,2}}{2}\right)^{1/2}\right\}\right.$$

$$+\frac{\sqrt{2\ s_2}}{q(V_2-V_3)}\left\{\left(q(V_2-V_3)+\frac{m\gamma^2}{2}\right)^{1/2} - \left(\frac{m\gamma^2}{2}\right)^{1/2}\right\}$$

$$\left.+\frac{s_3}{\left[mv_s^{\,2}+2q(V_s-V_3)\right]^{1/2}}\right]. \qquad (55)$$

Again, the relationship between t and m is quadratic, which is the anticipated result if we look upon this spectrometer as a "constant energy" device.

Spherical Two Field Spectrometer

One of the reasons that prompted the investigation of the cylindrical two field spectrometer was its nonlinear fields. How these fields influenced flight times and resolving power was unknown and seemed interesting. It is for this same reason that we shall now propose and theoretically consider a two field spectrometer of spherical geometry.

Figure 3 is a cross section of a spherical spectrometer consisting of three spherical grids and a spherical collecting plate. We again shall assume that positive ions are produced in or introduced into region 1 with some initial energy. The outer grid is periodically pulsed upward in potential from its normal potential V_2 to a potential $V_2 + P(t)$, thus producing an inwards acceleration of all ions in region 1. The pulse P(t) is maintained until all ions in region 1 have left. The ions starting from larger radii acquire more energy than those originating from smaller radii. The ions are further accelerated by the potential difference existing between grids two and three and enter region 3 which is again field free. In this region, the ions drift at constant velocity until they reach the collector which is at radius r_c.

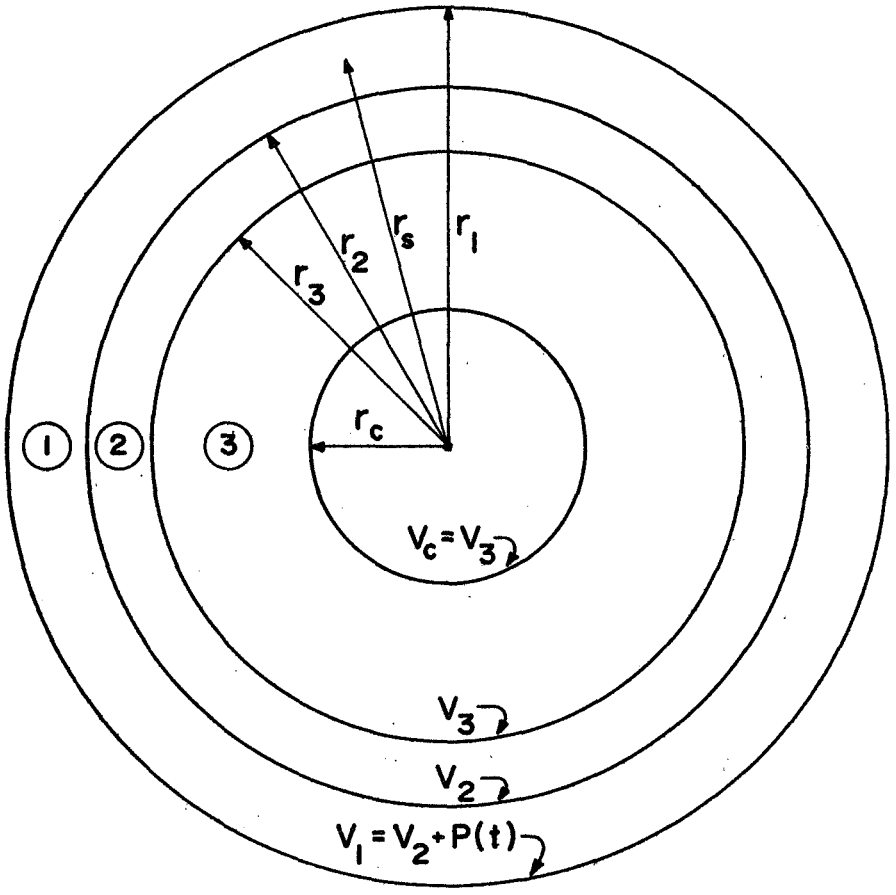

FIGURE 3. CROSS SECTION OF SPHERICAL TIME-OF-FLIGHT MASS SPECTROMETER WITH TWO ACCELERATING REGIONS

Following the pattern established in the two previous sections, we proceed to determine the relationship between mass and time as a function of the starting radii of the ions, of the radii and the potentials on the electrodes, and of ionic initial energies. Since regions 1 and 2 are geometrically and electrically similar, we shall use a generalized derivation to determine the time spent in a region such as these. We shall assume negligible charge density so that Laplace's equation can be used, and we shall consider only its radial term which is

$$\frac{1}{r}\frac{d^2}{dr^2}(rV) = 0 \tag{56}$$

which upon two successive integrations yields

$$V(r) = C_7 + \frac{C_8}{r} \quad . \tag{57}$$

Applying the boundary conditions results in

$$V_i = C_7 + \frac{C_8}{r_i} \tag{58}$$

$$V_j = C_7 + \frac{C_8}{r_j} \quad . \tag{59}$$

Solving for C_7 and C_8 gives

$$C_7 = \frac{r_j V_j - r_i V_i}{(r_j - r_i)} \tag{60}$$

$$C_8 = \frac{r_i r_j (V_i - V_j)}{(r_j - r_i)} \tag{61}$$

thus

$$V(r) = \frac{r_i r_j (V_i - V_j)}{(r_j - r_i) r} + \frac{r_j V_j - r_i V_i}{(r_j - r_i)} \quad . \tag{62}$$

The field then is

$$E(r) = \frac{r_i r_j (V_i - V_j)}{(r_j - r_i) r^2} \tag{63}$$

from which we can write the equation of motion

$$\frac{m d^2 r}{dt^2} = \frac{q r_i r_j (V_i - V_j)}{(r_j - r_i) r^2} \quad . \tag{64}$$

Multiplying both sides by dr/dt and integrating yields

$$\frac{1}{2}\left(\frac{dr}{dt}\right)^2 = \frac{-qr_i r_j (V_i - V_j)}{m(r_j - r_i)r} + C_9' \tag{65}$$

Rewriting equation (65) gives

$$\left(\frac{dr}{dt}\right)^2 = \frac{2q}{m}\ \frac{r_i r_j (V_i - V_j)}{(r_i - r_j)r} + C_9 \tag{66}$$

At $t = 0$, $r = r_0$ and $v = \pm v_0$; then

$$C_9 = v_0^2 - \frac{2q}{m}\ \frac{r_i r_j (V_i - V_j)}{(r_i - r_j)r_0} \tag{67}$$

so

$$\left(\frac{dr}{dt}\right)^2 = \left(\frac{2q}{m}\right)\ \frac{r_i r_j (V_i - V_j)}{(r_i - r_j)}\ \left(\frac{1}{r} - \frac{1}{r_0}\right) + v_0^2 \quad . \tag{68}$$

Let $K_{ij} = r_i r_j\ (V_i - V_j)/(r_i - r_j)$; then equation (68) becomes

$$\left(\frac{dr}{dt}\right)^2 = \left(\frac{2q}{m}\right) K_{ij}\ \left(\frac{1}{r} - \frac{1}{r_0}\right) + v_0^2 \quad . \tag{69}$$

Factoring 2q/m and taking the square root gives

$$\left(\frac{dr}{dt}\right) = \pm \left(\frac{2q}{m}\right)^{1/2} \left[K_{ij} \left(\frac{r_0 - r}{rr_0}\right) + \frac{mv_0^2}{2q}\right]^{1/2} . \tag{70}$$

Rewriting yields

$$\left(\frac{dr}{dt}\right) = \pm \left(\frac{2q}{m}\right)^{1/2} \left[\frac{K_{ij}(r_0 - r) + \frac{mv_0^2 rr_0}{2q}}{rr_0}\right]^{1/2} . \tag{71}$$

Arranging terms in r results in

$$\left(\frac{dr}{dt}\right) = \pm \left(\frac{2q}{m}\right)^{1/2} \left[\frac{r\left(\frac{mv_0^2 r_0}{2q} - K_{ij}\right) + K_{ij} r_0}{rr_0}\right]^{1/2} \tag{72}$$

and further factoring yields

$$\left(\frac{dr}{dt}\right) = \pm \left(\frac{2q}{m}\right)^{1/2} \frac{\left(\frac{mv_0^2 r_0}{2q} - K_{ij}\right)^{1/2}}{(rr_0)^{1/2}} \left[r + \frac{K_{ij} r_0}{\frac{mv_0^2 r_0}{2q} - K_{ij}}\right]^{1/2} . \tag{73}$$

Let

$$\gamma_{ij} = \frac{mv_0^2 r_0}{2q} - K_{ij} \tag{74}$$

and

$$\alpha_{ij} = \frac{K_{ij} r_0}{\gamma_{ij}} \quad , \tag{75}$$

then equation (73) becomes

$$\frac{dr}{dt} = \pm \left(\frac{2q}{m}\right)^{1/2} \frac{\gamma_{ij}^{1/2}}{(rr_0)^{1/2}} (r + \alpha_{ij})^{1/2} \, dr \, . \tag{76}$$

Separating the variables gives

$$\left(\frac{2q}{m}\right)^{1/2} dt = \pm \frac{(rr_0)^{1/2}}{\gamma_{ij}^{1/2}} (r + \alpha_{ij})^{-1/2} \, dr \, . \tag{77}*$$

We next make a MacLaurin's series expansion on $(r + \alpha_{ij})^{-1/2}$, thus

$$\left(\frac{2q}{m}\right)^{1/2} dt = \pm \frac{(rr_0)^{1/2}}{\gamma_{ij}^{1/2}} \sum_{n=0}^{\infty} \frac{r^n}{n!} \left[\frac{d^n (r+\alpha_{ij})^{-1/2}}{dr^h}\right]_{r=0} dr \, . \tag{78}$$

*If $r = w^2$ is chosen, $dt = 2(r_o/\gamma_{ij})^{1/2} \, w^2 dw/(w^2 + \alpha_{ij})^{1/2}$, which upon integration equals $(r_o/\gamma_{ij})^{1/2}(w\sqrt{w^2 + \alpha_{ij}} - \alpha_{ij} \, n(w + \sqrt{w^2 + \alpha_{ij}}))$.

If we consider the derivative terms in the series, it is quite easy to show that the relation

$$\left[\frac{d^n}{dr^n}\ (r + \alpha_{ij})^{-1/2}\right]_{r=0} = \frac{d^n(\alpha_{ij}^{-1/2})}{d\alpha_{ij}^{\ n}} \tag{79}$$

is true; consequently, equation (79) becomes

$$\left(\frac{2q}{m}\right)^{1/2} dt = \pm \left(\frac{r_0}{\gamma_{ij}}\right)^{1/2} \sum_{n=0}^{\infty} \frac{1}{n!}\ \frac{d^n\left(\alpha_{ij}^{-1/2}\right)}{d\alpha_{ij}^{\ n}}\ r^{n+1/2} dr \quad . \tag{80}$$

Integrating both sides yields

$$\left(\frac{2q}{m}\right)^{1/2} t = \pm \left(\frac{r_0}{\gamma_{ij}}\right)^{1/2} \sum_{n=0}^{\infty} \frac{1}{n!(n+3/2)}\ \frac{d^n\left(\alpha_{ij}^{-1/2}\right)}{d\alpha_{ij}^{\ n}}\ r^{n+3/2} + C_{10}. \tag{81}$$

At $t = 0$, $r = r_0$, therefore

$$C_{10} = \mp\left(\frac{r_0}{\gamma_{ij}}\right)^{1/2} \sum_{n=0}^{\infty} \frac{1}{n!(n+3/2)} \frac{d^n\left(\alpha_{ij}^{-1/2}\right)}{d\alpha_{ij}^{n}} r_0^{n+3/2}, \tag{82}$$

hence

$$\left(\frac{2q}{m}\right)^{1/2} t = \pm\left(\frac{r_0}{\gamma_{ij}}\right)^{1/2} \sum_{n=0}^{\infty} \frac{1}{n!(n+3/2)} \cdot$$

$$\frac{d^n\left(\alpha_{ij}^{-1/2}\right)}{d\alpha_{ij}^{n}} \left(r^{n+3/2} - r_0^{n+3/2}\right) \tag{83}$$

We are now in a position to determine the time of residence in the first two regions. In applying this equation to the first region, one has to be cautious. For the linear spectrometer, the solution of the equation of motion was such that effect of the initial velocity vectors toward or away from the collector was immediately apparent. Equation (83) is not of this type but similar to that of the cylindrical spectrometer. Although the

plus-minus sign appears in the equation, no plus-minus dependence on initial velocity is evident. In order to obtain the appropriate plus-minus dependence on initial velocity, the following two solutions must be written and have the form

$$\left(\frac{2q}{m}\right)^{1/2} t^{(N)} = \pm\left(\frac{r_0}{\gamma_{ij}}\right)^{1/2} \sum_{n=0}^{\infty} \frac{1}{n!(n+3/2)} \frac{d^n(\alpha_{ij}^{-1/2})}{d\alpha_{ij}^{n}} \cdot$$

$$(r^{n+3/2} - r_0^{n+3/2}) \tag{84a}$$

$$\left(\frac{2q}{m}\right)^{1/2} t^{(P)} = \pm\left(\frac{r_0}{\gamma_{ij}}\right)^{1/2} \sum_{n=0}^{\infty} \frac{1}{n!(n+3/2)} \frac{d^n(\alpha_{ij}^{-1/2})}{d\alpha_{ij}^{n}} \cdot$$

$$(r^{n+3/2} - r_0^{n+3/2}) \pm 2\left(\frac{r_0}{\gamma_{ij}}\right)^{1/2} \sum_{n=0}^{\infty} \frac{1}{n!(n+3/2)} \frac{d(\alpha_{ij}^{-1/2})}{d\alpha_{ij}^{n}}$$

$$(r^{*n+3/2} - r_0^{n+3/2}) \tag{84b}$$

where the superscripts N and P refer to negative and positive initial velocities respectively, where the choice of the plus or minus sign in each term will be discussed in succeeding paragraphs, and where r* is the position where all the initial kinetic energy of the ion has been transformed into potential energy. The factor of 2 in equation (84b) arises from the fact that twice the distance from r_0 to r* has to be traversed by the ion to bring it back to r_0 with a velocity vector oriented toward the collector. Before proceeding to the consideration of the specific regions, we must determine r*. Referring to equation (62) we can write the potential at r_0 and r*

$$V(r_0) = \frac{r_i r_j (V_i - V_j)}{(r_j - r_i) r_0} + \frac{r_j V_j - r_i V_i}{(r_j - r_i)} \tag{85}$$

$$V(r^*) = \frac{r_i r_j (V_i - V_j)}{(r_j - r_i) r^*} + \frac{r_j V_j - r_i V_i}{(r_j - r_i)} \quad . \tag{86}$$

The relation between $V(r_0)$ and V(r*) is simply

$$V(r^*) = V(r_0) + \frac{1}{2} \frac{m v_0^2}{q} \quad . \tag{87}$$

Using equations (85), (86), and (87), we get

$$\frac{r_i r_j (V_i - V_j)}{(r_j - r_i) r^*} = \frac{r_i r_j (V_i - V_j)}{(r_j - r_i) r_0} + \frac{1}{2} \frac{m v_0^2}{q} \quad . \tag{88}$$

Factoring yields

$$\frac{1}{r^*} = \frac{1}{r_0} + \frac{m v_0^2 (r_j - r_i)}{2q r_i r_j (V_i - V_j)} \tag{89}$$

which upon taking the reciprocal becomes

$$r^* = \frac{1}{\frac{1}{r_0} + \frac{m v_0^2 (r_j - r_i)}{2q r_i r_j (V_i - V_j)}} \tag{90}$$

Considering region 1, $v_0 = \pm v_s$, $r_i = r_1$, $r_j = r_2$, $r_0 = r_s$; thus,

$$K_{12} = \frac{r_1 r_2 (V_1 - V_2)}{r_1 - r_2} \tag{91}$$

$$\gamma_{12} = \frac{m v_s^2 r_s}{2q} - \frac{r_1 r_2 (V_1 - V_2)}{r_1 - r_2} \tag{92}$$

$$\alpha_{12} = \frac{r_1 r_2 r_s (V_1 - V_2)}{(r_1 - r_2)\left[\frac{m v_s^2 r_s}{2q} - \frac{r_1 r_2 (V_1 - V_2)}{r_1 - r_2}\right]} . \tag{93}$$

α_{12} can be rewritten as

$$\alpha_{12} = \frac{r_s r_1 r_2 (V_1 - V_2)}{\frac{m v_s^2 r_s (r_1 - r_2)}{2q} - r_1 r_2 (V_1 - V_2)} . \tag{94}$$

For an ion with a negative initial radial velocity, i.e., toward the center of the spectrometer,

$$T_1^{(n)} = -\left(\frac{m}{2q}\right)^{1/2} \left(\frac{r_s}{\alpha_{12}}\right)^{1/2} \sum_{n=0}^{\infty} \frac{1}{n!(n+3/2)} \frac{d^n(\alpha_{12}^{-1/2})}{d\alpha_{12}^n} .$$

$$(r_2^{n+3/2} - r_s^{n+3/2}) \tag{95}$$

where the superscript $\underline{n}$ refers to the negative radial velocity and the minus sign is chosen because $r_2 < r_s$. For an ion with a positive initial radial velocity, i.e., away from the center of the spectrometer,

$$T_1^{(p)} = -\left(\frac{m}{2q}\right)^{1/2} \left(\frac{r_s}{\gamma_{12}}\right)^{1/2} \sum_{n=0}^{\infty} \frac{1}{n!(n+3/2)} \frac{d^n\left(\alpha_1^{-1/2}\right)}{d\alpha_{12}^{\,n}}$$

$$\left(r_2^{\,n+3/2} - r_s^{\,n+3/2}\right) + 2\left(\frac{m}{2q}\right)^{1/2} \left(\frac{r_s}{\gamma_{12}}\right)^{1/2} .$$

$$\sum_{n=0}^{\infty} \frac{1}{n!(n+3/2)} \frac{d^n\left(\alpha_{12}^{-1/2}\right)}{d\alpha_{12}^{\,n}} \left(r^{*n+3/2} - r_s^{\,n+3/2}\right) \tag{96}$$

where the superscript (p) refers to the positive radial velocity, the minus sign is chosen in the first term because $r_2 < r_s$, the positive sign is chosen in the second term because $r^* > r_s$ and r^* is given by equation (97)

$$r^* = \frac{1}{\frac{1}{r_s} + \frac{mv_0^2(r_2-r_1)}{2qr_1r_2(V_1-V_2)}} \quad . \tag{97}$$

For region 2, $r_i = r_2$, $r_j = r_3$ and $r_0 = r_2$. v_0^2 for the second region can be found from equation (98)

$$v_0^2 = v_s^2 + \frac{2q}{m}(V_s-V_2) = \xi^2 \tag{98}$$

where according to equation (62)

$$V_s = \frac{r_1r_2(V_1-V_2)}{(r_2-r_1)r_s} + \frac{r_2V_2-r_1V_1}{(r_2-r_1)} \quad . \tag{99}$$

Also,

$$K_{23} = \frac{r_2r_3(V_2-V_3)}{r_2-r_3} \tag{100}$$

$$\gamma_{23} = \frac{m\xi^2 r_2}{2q} - \frac{r_2 r_3 (V_2 - V_3)}{r_2 - r_3} \tag{101}$$

$$\alpha_{23} = \frac{r_2^2 r_3 (V_2 - V_3)}{\frac{m\xi^2 r_2 (r_2 - r_3)}{2q} - r_2 r_3 (V_2 - V_3)} \quad . \tag{102}$$

Thus,

$$T_2 = -\left(\frac{m}{2q}\right)^{1/2} \left(\frac{r_2}{\gamma_{23}}\right)^{1/2} \sum_{n=0}^{\infty} \frac{1}{n!\, n+3/2} \frac{d^n(\alpha_{23}^{-1/2})}{d\alpha_{23}^{n}} \quad .$$

$$\left(r_3^{n+3/2} - r_2^{n+3/2}\right) \tag{103}$$

where the minus sign was chosen because $r_3 < r_2$ and the second term in the generalized solution is equal to zero since $r^* = r_2$, i.e., only negative radial velocities are allowed in region 2.

Since region 3 is field free, we can quickly determine the time spent in this region by dividing the radial length of the region by the velocity of the ion upon entry into this region. The velocity squared is given by

$$v_0^2 = v_s^2 + \frac{2q}{m}(V_s - V_3) \tag{104}$$

where V_s has already been defined by equation (99). Thus, the time spent in region 3 is

$$T_3 = \left(\frac{m}{2q}\right)^{1/2} \frac{r_3 - r_c}{\left(\frac{mv_s^2}{2q} + (V_s - V_3)\right)^{1/2}} \cdot \tag{105}$$

To determine the total time of flight of an ion starting at radius r_s with a negative initial radial velocity, equations (95), (103) and (105) must be summed yielding

$$T_t(n) = \left(\frac{m}{2q}\right)^{1/2} \left\{ -\left(\frac{r_s}{\gamma_{12}}\right)^{1/2} \sum_{n=0}^{\infty} \frac{1}{n!(n+3/2)} \frac{d^n\left(\alpha_{12}^{-1/2}\right)}{d\alpha_{12}^{n}} \cdot \right.$$

$$\left(r_2^{n+3/2} - r_s^{n+3/2}\right) - \left(\frac{r_s}{\gamma_{23}}\right)^{1/2} \sum_{n=0}^{\infty} \frac{1}{n!(n+3/2)} \cdot$$

$$\frac{d^n\left(\alpha_{23}^{-1/2}\right)}{d\alpha_{23}^{n}} \left(r_3^{n+3/2} - r_2^{n+3/2}\right)$$

$$\left. + \frac{r_3 - r_c}{\left(\frac{mv_s^2}{2q} + V_s - V_3\right)^{1/2}} \right\} \qquad (106)$$

To determine the total flight time of an ion starting at radius r_s with a positive initial radial velocity, equations (96), (103) and (105) are summed resulting in

$$T_t^{(p)} = \left(\frac{m}{2q}\right)^{1/2} \left\{ -\left(\frac{r_s}{\gamma_{12}}\right)^{1/2} \sum_{n=0}^{\infty} \frac{1}{n!(n+3/2)} \frac{d^n(\alpha_{12}^{-1/2})}{d\alpha_{12}^n} \right.$$

$$(r_2^{n+3/2} - r_s^{n+3/2}) + 2\left(\frac{r_s}{\gamma_{12}}\right)^{1/2} \sum_{n=0}^{\infty} \frac{1}{n!n+3/2}$$

$$\frac{d^n(\alpha_{12}^{-1/2})}{d\alpha_{12}^n} \quad (r^{*n+3/2} - r_s^{n+3/2})$$

$$-\left(\frac{r_2}{\gamma_{23}}\right)^{1/2} \frac{1}{n!(n+3/2)} \frac{d^n(\alpha_{12}^{-1/2})}{d\alpha_{23}^n} \quad (r_3^{n+3/2} - r_2^{n+3/2})$$

$$\left. + \frac{r_3 - r_c}{\left(\frac{m v_s^2}{2q} + V_5 V_3\right)^{1/2}} \right\} \qquad (107)$$

Interpretation

In order to analyze the ion focusing properties of the cylindrical, linear, and spherical spectrometers, computer programs were written to determine the flight times of ions as a function of the starting positions, of ratios of voltages on the first and second electrodes, and of the initial velocities of the ions for several sets of spectrometer dimensions.

The ion focusing properties of interest are space focusing and energy focusing. Space focusing exists when ions despite their initial spatial distribution in the pulsed region arrive at the collector within a relatively short time of each other. Energy focusing exists when the time spread introduced by the initial kinetic energies of the ions is minimized.

A study of space focusing can be made by setting the initial ion energy spread equal to zero, thus eliminating from consideration the requirements of energy focusing which are generally in conflict with those of space focusing. Figure 4 shows a family of curves of $(2q/m)^{1/2}$ times the flight time versus the starting positions which are available in the pulsed region of a cylindrical spectrometer. The dimensions of the spectrometer under analysis are $r_1 = 9.00$ cm., $r_2 = 8.50$ cm., $r_3 = 8.20$ cm., and $r_c = 4.60$ cm. These dimensions were chosen such as to be compatible with the volume available on the flight instrumentation package. Each curve is drawn for a constant ratio $\underline{R}$ of V_1 to V_2 where V_2 has

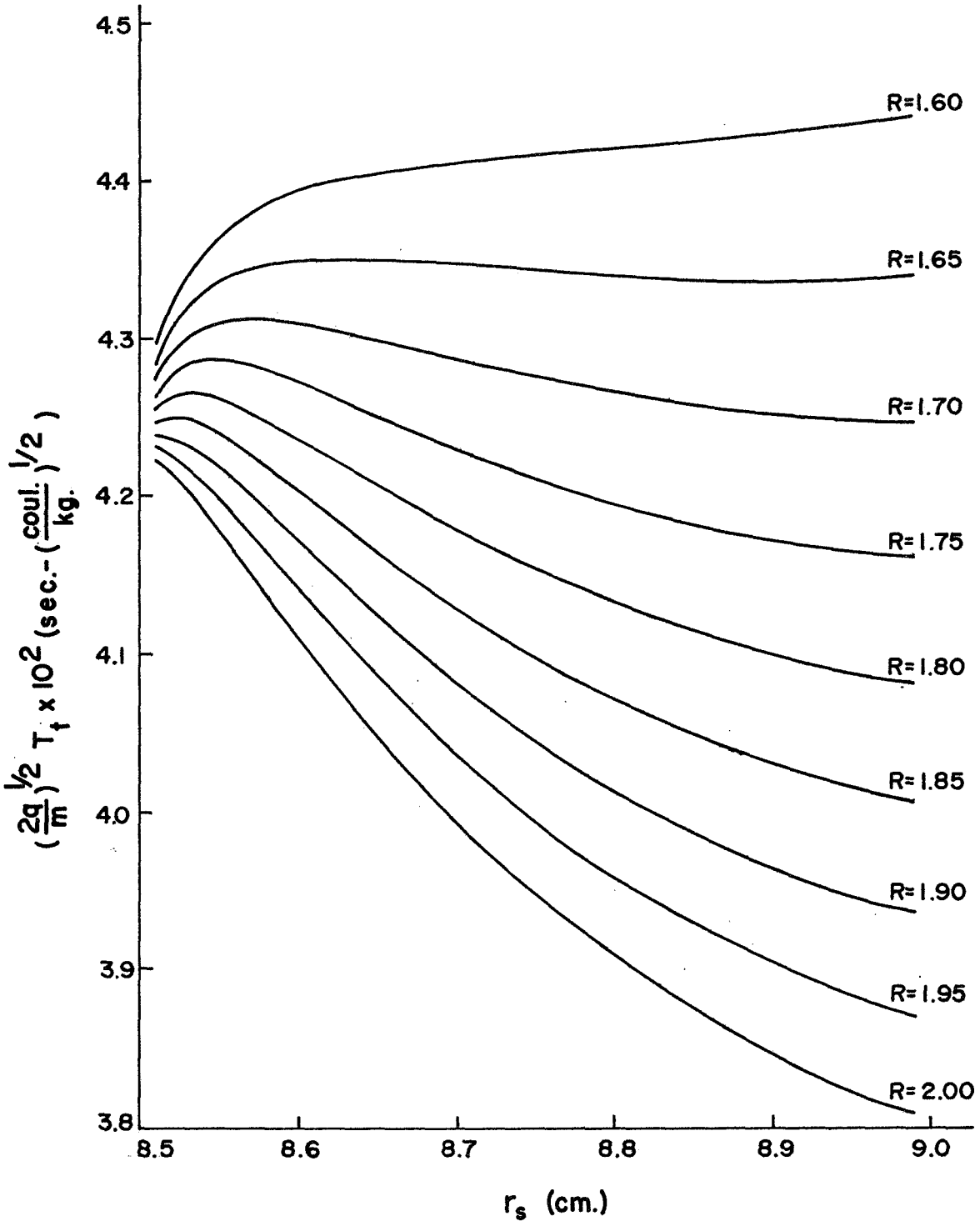

FIGURE 4. SPACE FOCUSING CHARACTERISTICS OF A CYLINDRICAL MASS SPECTROMETER WITH r_1=9.00cm., r_2=8.50cm., r_3=8.20cm., AND r_c=4.60cm.

been set equal to 1 volt and V_3 to 0 volts. As can be seen, the voltage ratio V_1/V_2 of approximately 1.65 displays the best focusing. At this ratio, 90 percent of the ions arrive at the collector within a short interval of time.

With the dimensions of region 1 set in order to maintain the highest possible sensitivity, i.e., the largest available pulsing region volume, the radial dimension of region 2 was altered by varying r_3. First, r_3 was increased from 8.30 cm. to 8.45 cm. This increase in r_3 increased the time spent in the field free region and reduced the time spent by the ions in reaching their terminal energies. Both of these things seemed intuitively desirable. The results are shown in figures 5, 6, and 7. These, however, show no dramatic change in space focusing. The flatness of the best focusing curves in these figures is comparable and the range of starting positions over which best focusing occurs is approximately equal. However, it should be noted that the voltage ratio at which best focusing occurs increases as the value of r_3 increases.

Since no significant increase in space focusing occurred by increasing r_3, r_3 was decreased. The decreases in r_3 were limited because energy focusing, which shortly will be discussed, requires that the ions reach their terminal energies as quickly as possible. Figures 8 and 9 indicate the space focusing characteristics for spectrometers with r_3 = 8.10 cm. and r_3 = 8.00 cm. respectively. Again, no significant change in the quality of focusing was obtained.

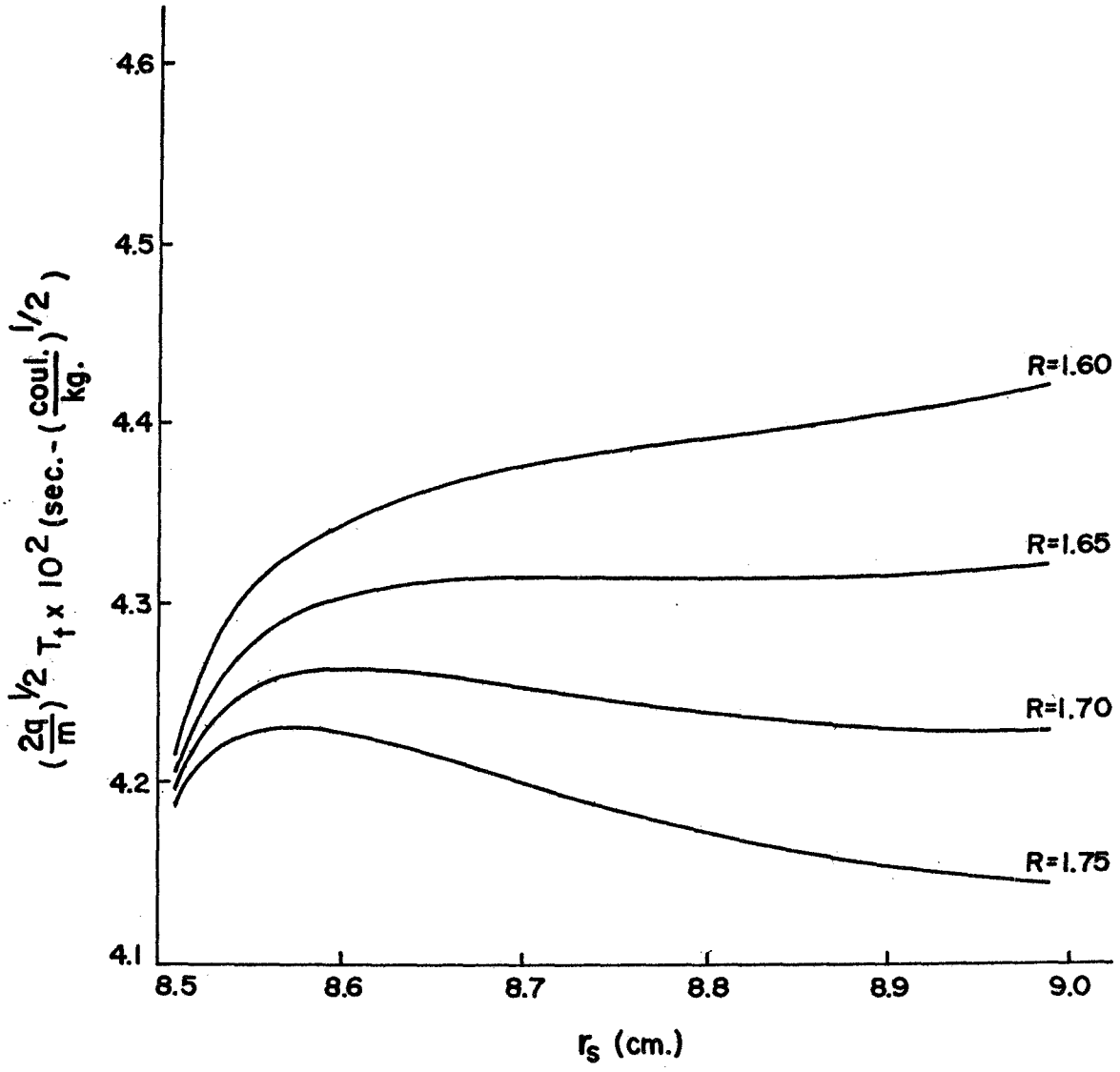

FIGURE 5. SPACE FOCUSING CHARACTERISTICS OF A CYLINDRICAL MASS SPECTROMETER WITH r_1 = 9.00 cm., r_2 = 8.50 cm., r_3 = 8.30 cm., AND r_c = 4.60 cm.

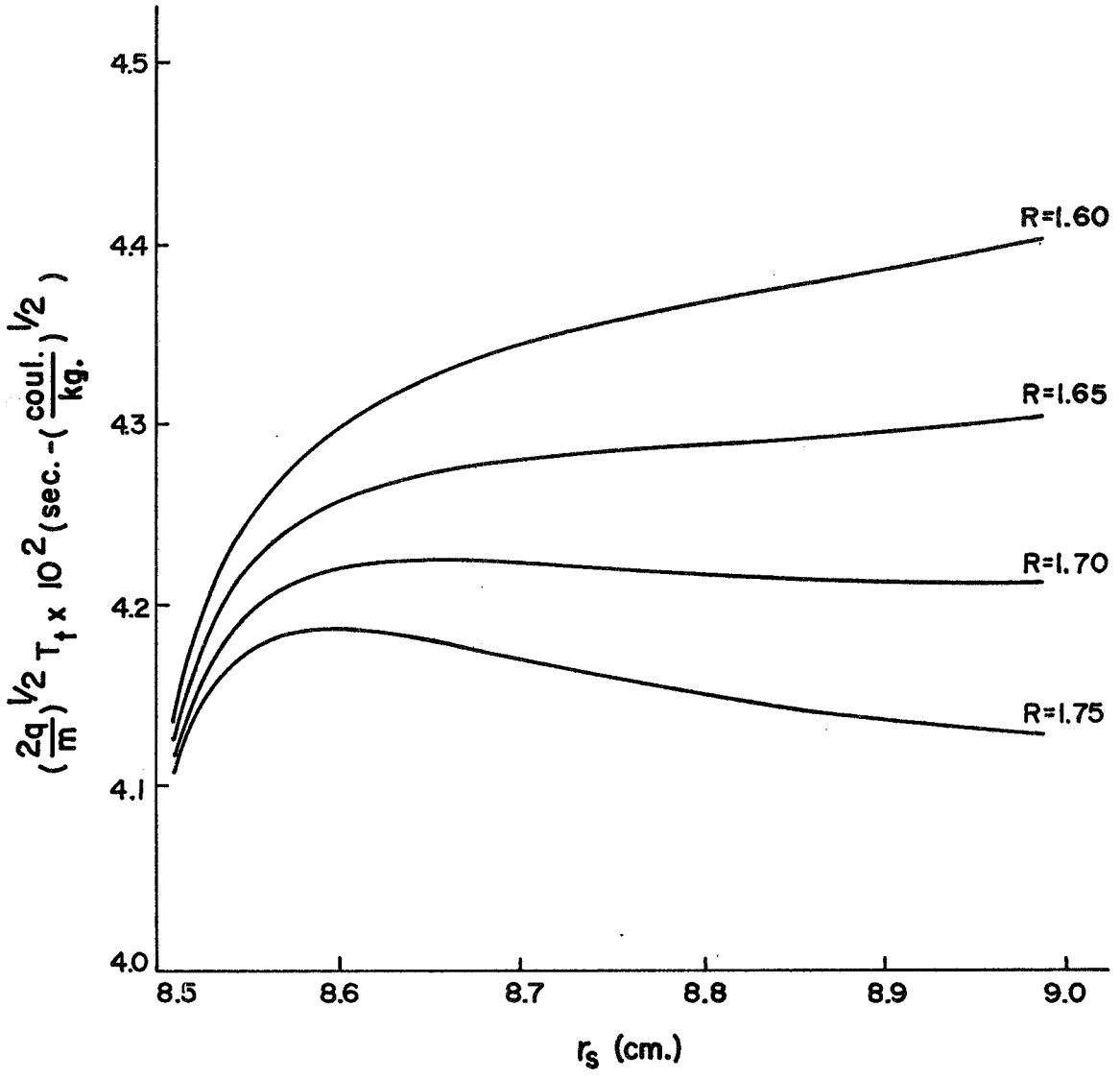

FIGURE 6. SPACE FOCUSING CHARACTERISTICS OF A CYLINDRICAL MASS SPECTROMETER WITH $r_1 = 9.00$ cm., $r_2 = 8.50$ cm., $r_3 = 8.40$ cm., AND $r_c = 4.60$ cm.

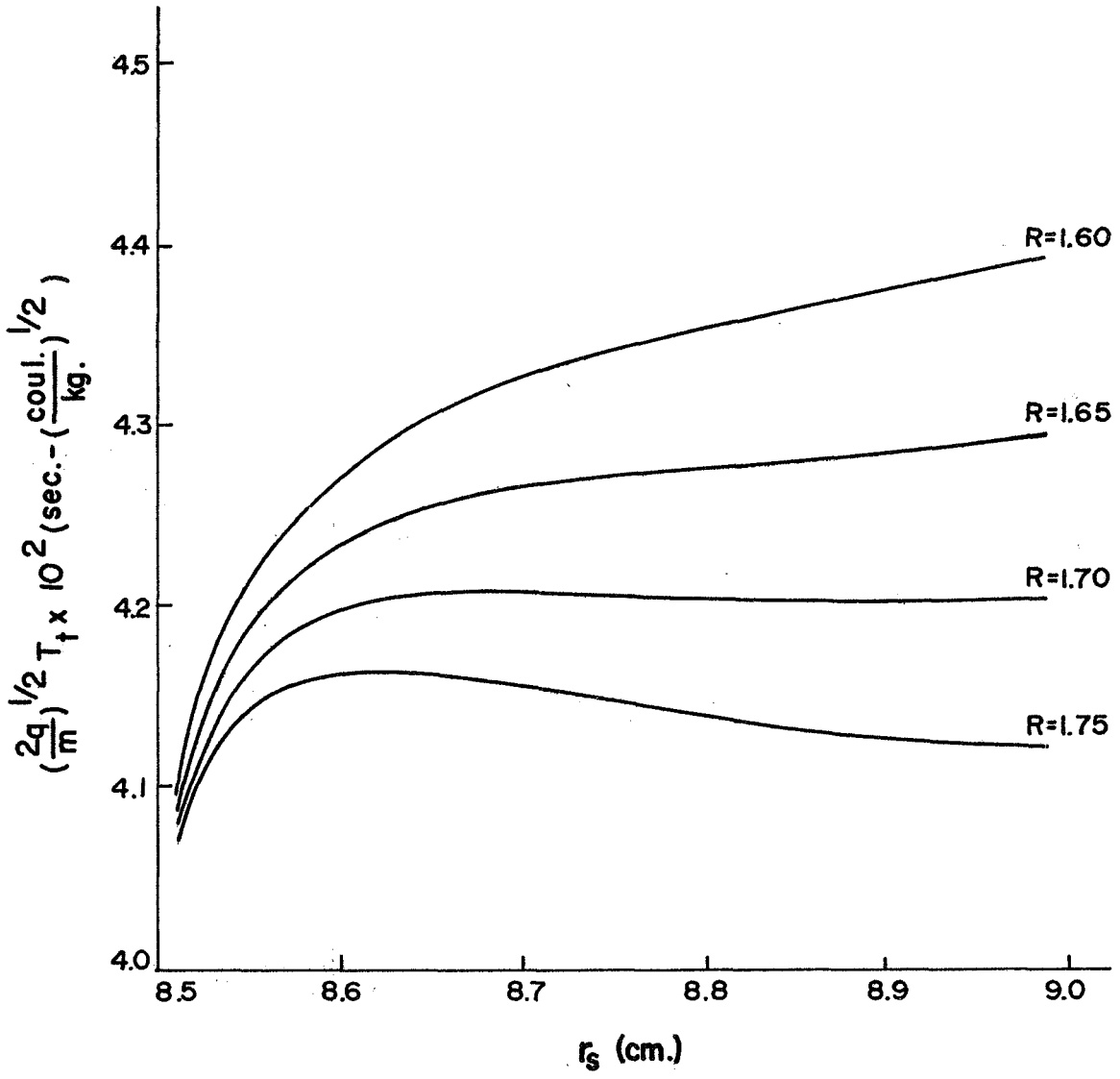

FIGURE 7. SPACE FOCUSING CHARACTERISTICS OF A CYLINDRICAL MASS SPECTROMETER WITH $r_1 = 9.00$ cm., $r_2 = 8.50$ cm., $r_3 = 8.45$ cm., AND $r_c = 4.60$ cm.

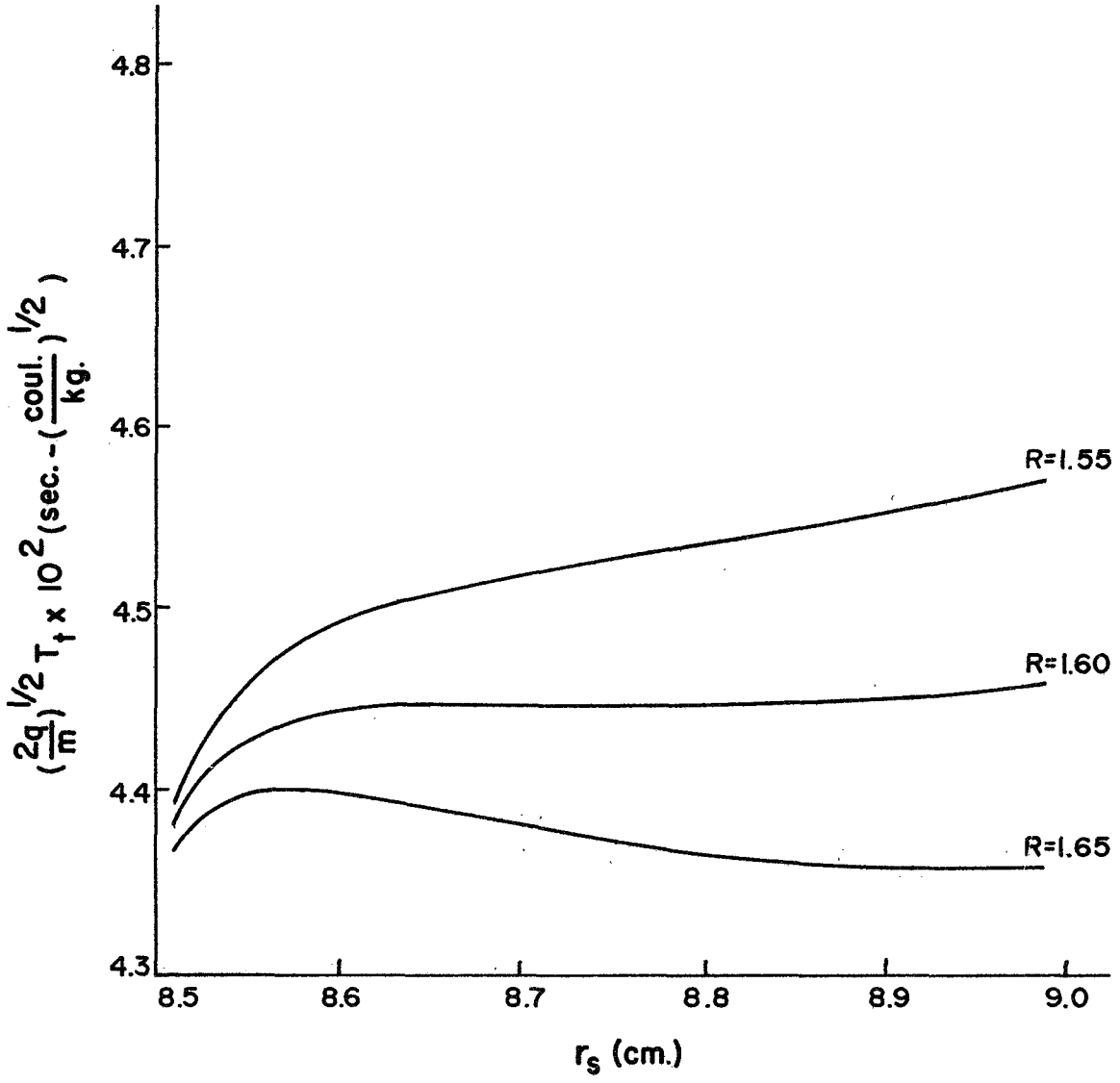

FIGURE 8. SPACE FOCUSING CHARACTERISTICS OF A CYLINDRICAL MASS SPECTROMETER WITH $r_1 = 9.00$ cm., $r_2 = 8.50$ cm., $r_3 = 8.10$ cm., AND $r_c = 4.60$ cm.

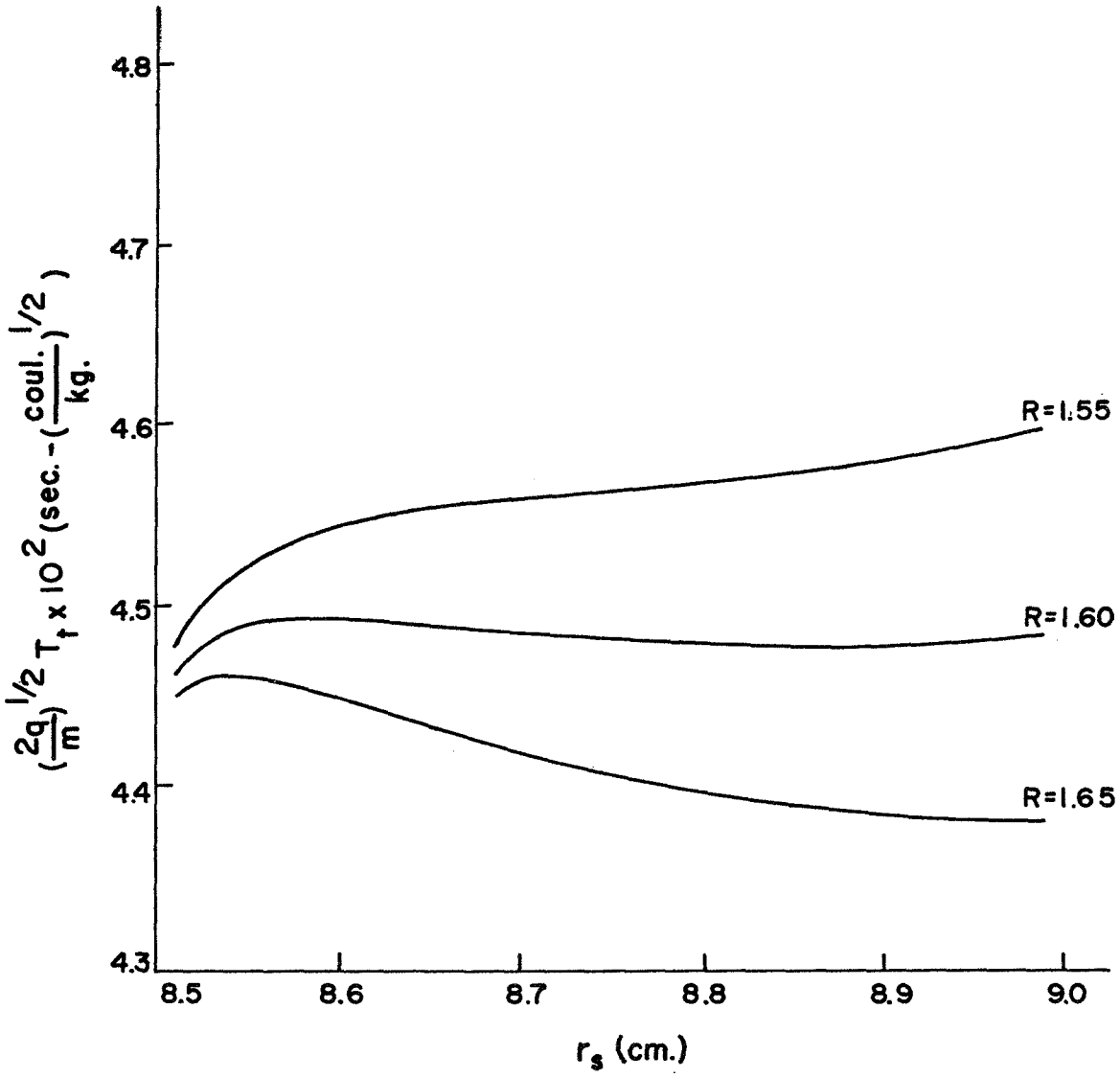

FIGURE 9. SPACE FOCUSING CHARACTERISTICS OF A CYLINDRICAL MASS SPECTROMETER WITH $r_1 = 9.00$ cm., $r_2 = 8.50$ cm., $r_3 = 8.00$ cm., AND $r_c = 4.60$ cm.

Since no particular value of r_3 possessed any significant space focusing advantage, other considerations became the deciding factors in the choice of r_3. The vibrations encountered during a rocket flight made the choice of a smaller r_3 more desirable. However, r_3 could not be made too small due to energy focusing requirements. Consequently, r_3 was chosen to be 8.20 cm. in the flight instrument because it met all the apparent requirements.

In order to determine the relative merits of the cylindrical spectrometer, the linear spectrometer was chosen as the norm. The dimensions of the linear device were chosen identical to the cylindrical device, namely, the lateral dimensions of regions 1, 2, and 3, were 0.5 cm., 0.3 cm., and 3.6 cm. Figure 10 shows curves of $(2q/m)^{1/2}$ times the flight time versus starting position. It can be seen that ions from only about 75 percent of the pulsing region are reasonably focused. It should be noted that the voltage ratio for optimum performance is lower. Also, if figure 10 is superimposed on figure 4, it will be seen that small variations off the optimum conditions for the cylindrical case are not as deleterious to performance as for the linear case.

For the spherical configuration, a similar analysis has been performed. This analysis is oriented as the basis for future study since the construction of such a device which is truly uniformly spherical and capable of withstanding a rocket launch is not a simple task. Figure 11 shows the results of the analysis. The axes used in this figure are the same as those used in figures 4

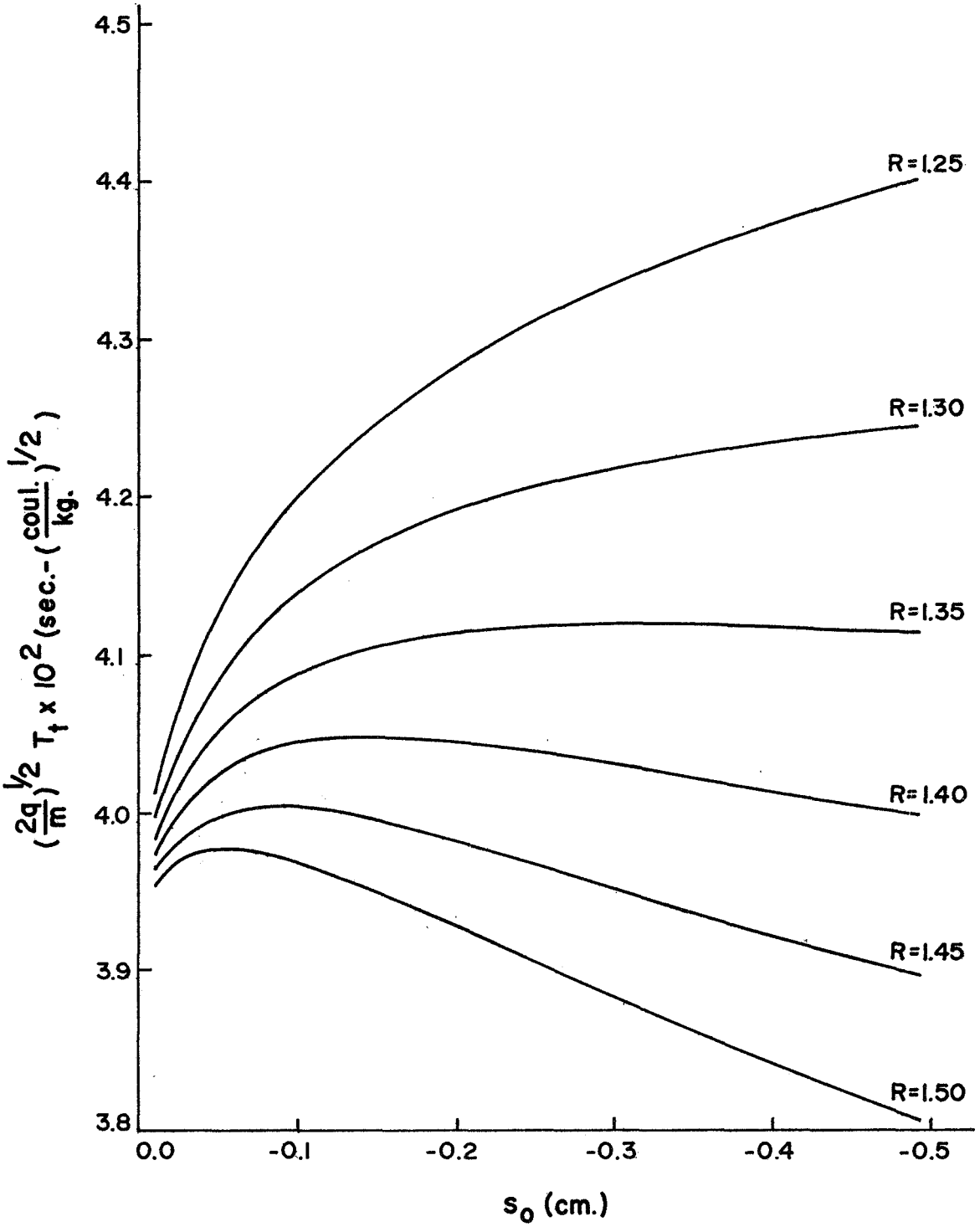

FIGURE 10. SPACE FOCUSING CHARACTERISTICS OF A LINEAR MASS SPECTROMETER WITH s_1= 0.5 cm., s_2= 0.3 cm., AND s_3= 3.6 cm.

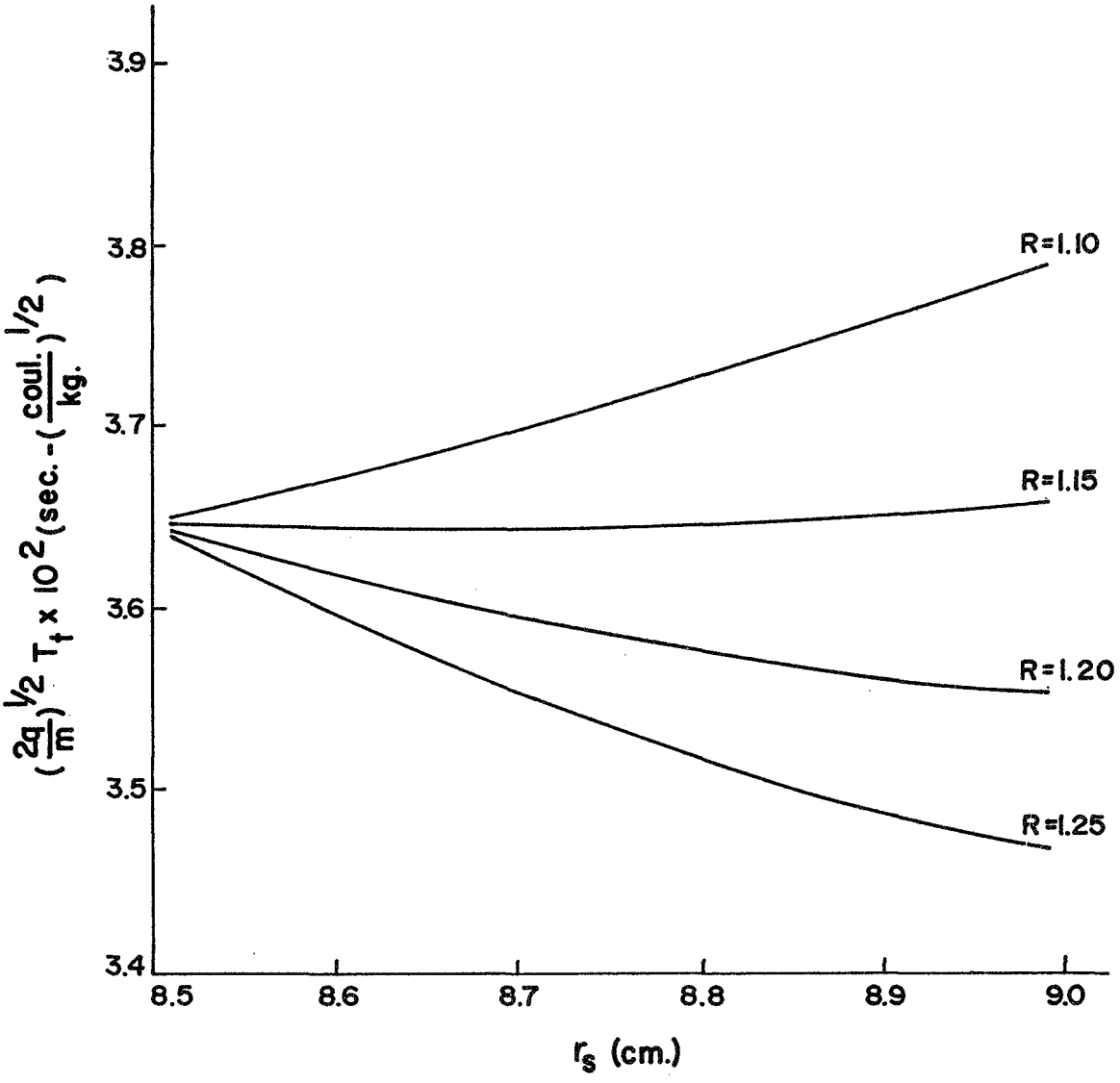

FIGURE II. SPACE FOCUSING CHARACTERISTICS OF A SPHERICAL MASS SPECTROMETER WITH $r_1 = 9.00$ cm., $r_2 = 8.50$ cm., $r_3 = 8.20$ cm., AND $r_c = 4.60$ cm.

through 10. The grid and collector radii were chosen to be identical with those of the flight cylindrical spectrometer. The space focusing here seems to be the best of all configurations that have been considered. Ions are well focused from about 96 percent of the pulsing region. Another promising feature of this design is the low voltage ratio at which focusing occurs. This feature would alleviate some of the experimental difficulties encountered with the cylindrical design, namely, high voltage pulses (~80V). Some of these difficulties will be discussed in the experimental section of this work.

Energy focusing places opposite demands on the optimum voltage ratio (Wiley and McLaren, 1955). The primary methods of achieving good energy focusing are to accelerate the ions to their maximum velocities in the shortest time possible so that their time averaged energies are approximately the energies gained from the field and to make the energies acquired from the fields much greater than their initial energies. The first method implies making the two accelerating regions very small. Making both these regions small introduces the possibility of contact between adjacent electrodes, thus short circuiting. Also, the size of the pulsing region is governed by the sensitivity required for useful ionospheric work. The second method is limited by the possibility of discharging between adjacent electrodes or between electrodes and support structures.

Figure 12 shows curves of $(2q/m)^{1/2}$ times the flight time versus starting position for a cylindrical spectrometer. The radii used in this calculation were r_1 = 9.00 cm., r_2 = 8.50 cm., r_3 = 8.20 cm., and r_c = 4.60 cm. The ratio R was varied from 2.20 to 2.35 with V_2 equal to 60.0 volts and V_3 equal to zero volts. The initial ion energy was set at 1.50 eV. The upper family of curves is for those ions with an initial positive radial velocity and the lower family of curves is for those ions with an initial negative radial velocity. This initial energy and the values of V_2 and V_3 are experimentally typical. Figure 13 is a graph of the time spread ΔT time $(2q/m)^{1/2}$ versus the ratio R. This time spread is defined by the difference between the longest and shortest flight times for ions with starting positions ranging from 8.51 cm. to 8.99 cm. and for the spectrometer parameters given in figure 12. For this particular spectrometer, it is seen in figure 4 that the optimum space focusing value for R was 1.65. However, on the basis of the data presented in figure 13, it is obvious that R equal to 1.65 is not the best ratio for maximum resolving power. As was expected, the time spread decreases as R increases; however, this is certainly not a linear relationship. It should be mentioned, also, that as R is increased so are the experimental difficulties such as discharge phenomena, spectral frequencies too high for detector circuits, and the design and construction of high voltage pulse circuits which are suitable for rocket flight. One is

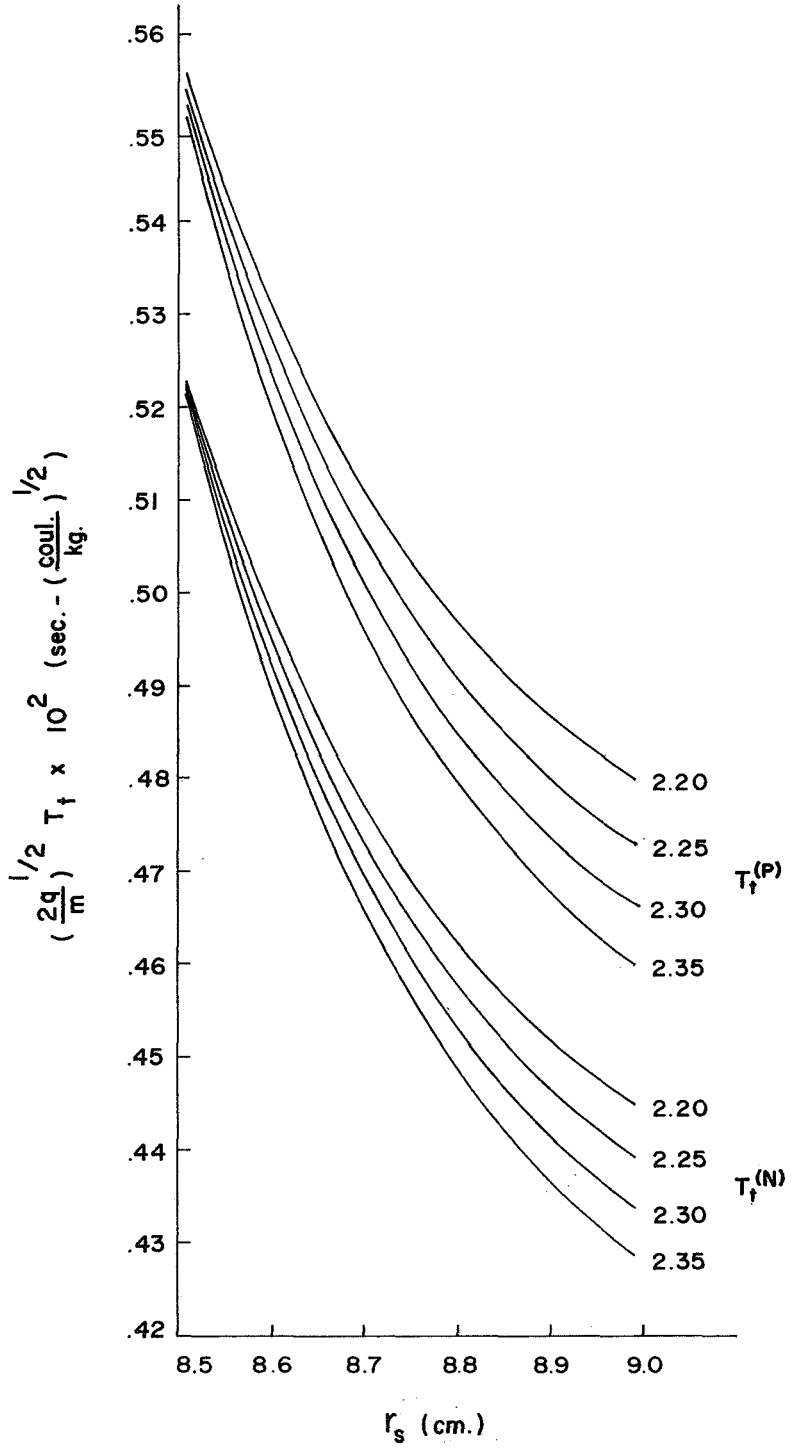

FIGURE 12. FLIGHT TIMES vs. STARTING POSITION FOR IONS WITH AN INITIAL ENERGY IN A CYLINDRICAL MASS SPECTROMETER

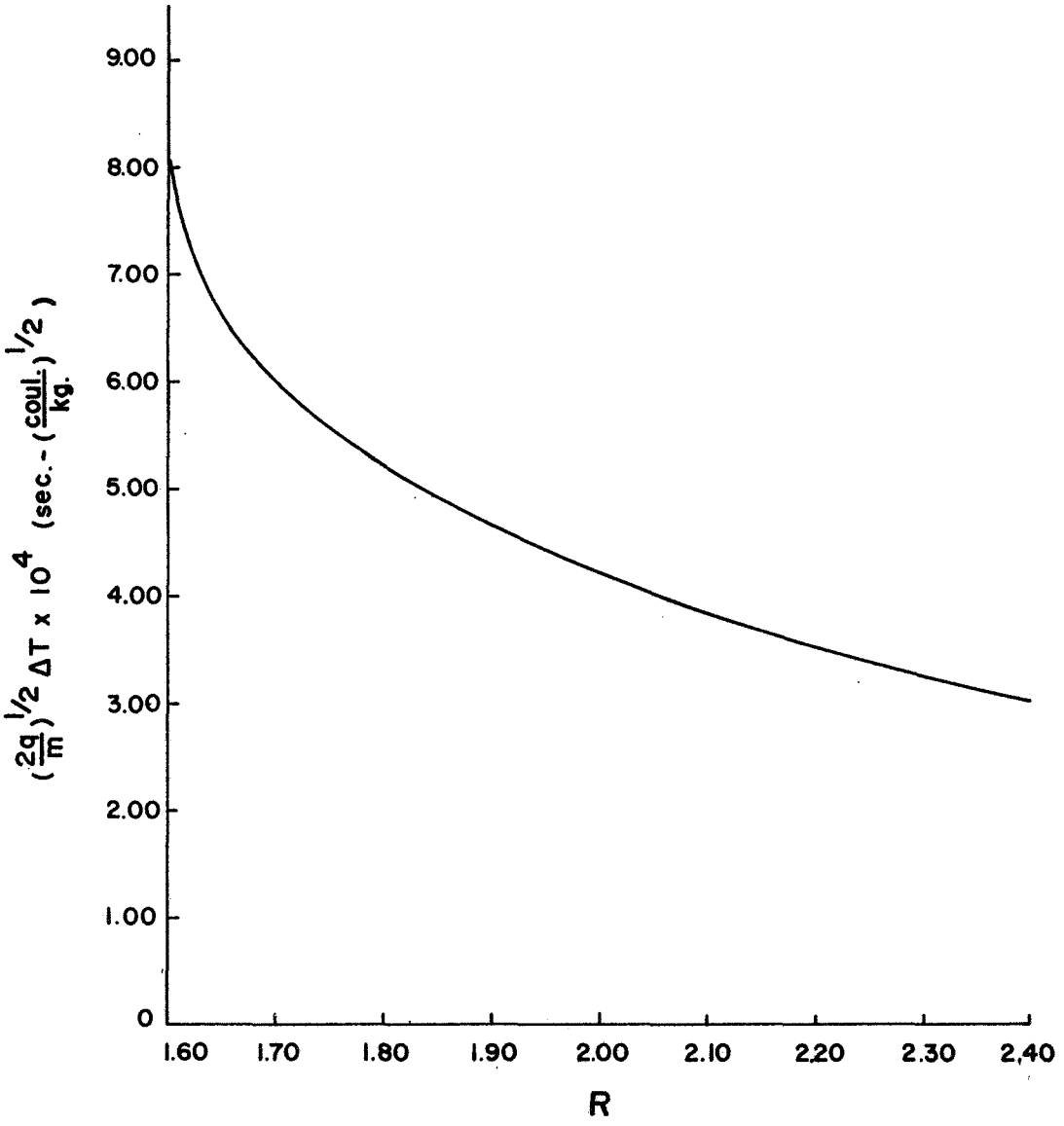

FIGURE 13. TIME SPREAD vs. VOLTAGE RATIO FOR A CYLINDRICAL MASS SPECTROMETER ANALYZING IONS WITH AN INITIAL ENERGY

tempted to define a term called "resolving power yield" which is simply $(-d\Delta T/dr)$. From the trend in figure 13, it can be seen that this term will become small for large values of R.

An alternate method to increasing R is to increase the potential difference between the second and third electrodes. However, this introduces some of the same difficulties that are introduced by increasing R, namely, discharge events, high spectral frequencies, and high voltage circuits. Also, since the ions spend more time in the pulsing region than in the second region, increasing the potential difference between the second and third electrodes has less influence on the time averaged energies of the ions than increasing R.

Line Shape Considerations

The space focusing curves that have been presented allow the computation of the true line shape of the instrument without the distortions introduced by the initial energy spread of the ions. This true line shape can be determined from the following considerations. It is of interest to find the current $i(T_t, r_s)$ which reaches the collector. For the cylindrical case, under the assumption of zero initial kinetic energy, the amount of charge present in a differential volume element is

$$dq(T_t,r_s) = 2\pi ehn(r_s)r_s(T_t)dr_s \qquad (108)$$

where $n(r_s)$ is the ion number density at $r_s(T_t)$, $r_s(T_t)$ is the starting position of the ions which have a particular flight time T_t; e is the basic electronic charge, and h is the height of the cylinder. Since current is simply dq/dt, then

$$i(T_t,r_s) = 2\pi ehn(r_s)r_s(T_t)\frac{dr_s}{dT_t} \tag{109}$$

It should be noted here that dr_s/dT_t is not an ion velocity but a derivative of a space focusing curve. From the curves that have been presented, it has been seen that for a given value of T_t, ions from more than one differential volume element can arrive at the collector. To account for this possibility, a summation of currents must be performed; hence, equation (109) must be written

$$i(T_t,\sum_j r_{sj}) = 2\pi eh\sum_j n(r_{sj})r_{sj}(T_t)\left.\frac{dr_s}{dT_t}\right|_{r_{sj}} \tag{110}$$

The broad line shape in figure 14 is a line shape for cylindrical mass spectrometer with V_2 = 60.0 volts, V_3 = 0.0 volts, and R = 2.40. The range of starting radii and the grids' and collector's radii are the same as those used in figure 12. The ordinate of this graph is $i(T_t,\sum_j r_{sj})/2\pi ehn$ where $n(r_s)$ = n which is a constant, i.e., a uniform ion concentration over the pulsing region has been assumed. The abscissa is $(2q/m)^{1/2}\ T_t$. For this

value of R, a semi-rectangular line shape has been obtained. It can be seen that the top of this shape has a negative slope. If R had been chosen below the optimum space focusing R, this slope would have been positive. Because no ions from different starting positions arrived at the collector at the same time, a smooth line shape top was obtained. On the other hand, if R is set to 1.65, the optimum space focusing value, the line shape no longer has this smooth top. This optimum line shape has a width at its base which is 1/6 that of the shape with R = 2.40. If along one radius the pulsing region is divided into a thousand equal elements and into each element one proton is placed, then typically two to four protons arrive at the collector within approximately 7 picoseconds of each other when R = 1.65. Also, there are instances when 15 to 30 ions arrive within this time interval and in one instance 62 ions arrive within this interval. To present all the detailed structure of the line shape at R = 1.65 is not possible within the allotted format of this work, so that what is presented in figure 14 is a line shape which would be expected from a detector with a frequency response less than that required to show all the structure.

In order to determine the actual line shape when an initial energy spread exists, a conceptually simple but computationally tedious method must be used. Given the energy distribution, all the line shapes must be computed for all the energies in the

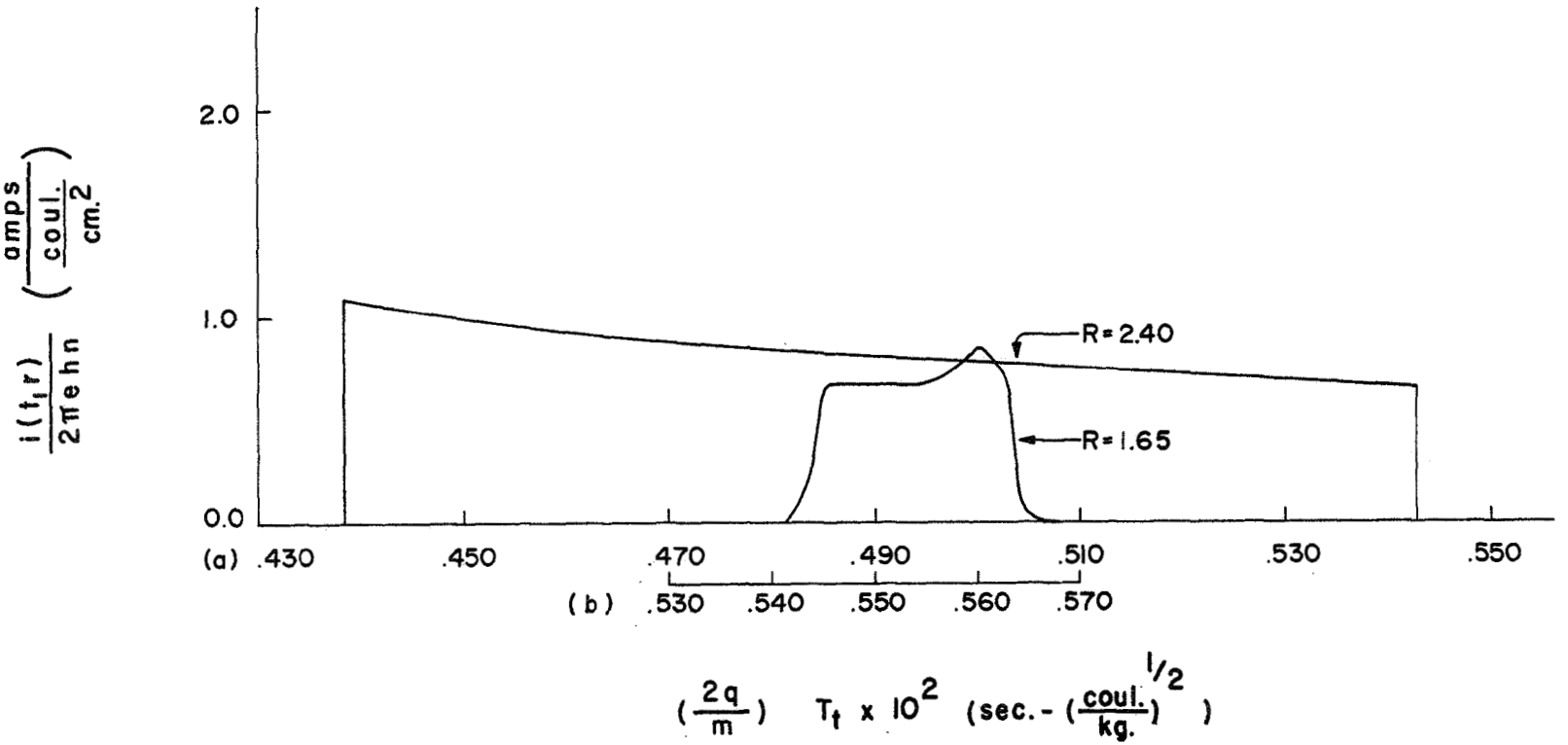

FIGURE 14. CYLINDRICAL MASS SPECTROMETER LINE SHAPES ASSUMING NO INITIAL ION ENERGY SPREAD
(a) R=2.40 (b) R=1.65

distribution. Next, each line shape must be weighted by the probability for that energy existing. After weighting, then all the line shapes must be summed.

III. EXPERIMENTAL CONSIDERATIONS

General Instrument Description

As has already been stated, the primary motivation for the investigation of the cylindrical time-of-flight mass spectrometer was the development of an instrument to measure the ion composition in the D-region. In order to give the instrument package the capability of being launched from installations located in remote as well as easily accessible locations, a small rocket was chosen as the vehicle. This capability was bought with the reduction of package weight and size. The size constraint made the choice of a cylindrical wedge the most desirable. Figure 15 is a photograph of the instrument. This geometrical configuration provided the best sensitivity per unit volume of package and the longest possible flight path. The angle of the wedge was 46°, the radial dimensions were r_1 = 9.00 cm., r_2 = 8.50 cm., r_3 = 8.20 cm., r_c = 4.40 cm., and the height of the wedge was 4.76 cm. The volume of the pulsing region was 17.15 cm^3. The unused region below the collector was removed in the flight version. The three extra grids located at 1 mm. intervals of each other, the last of which is located 1 mm. from the collector, constitute an ion gate system which shall be discussed shortly.

Electronics

In the theoretical presentation, we introduced the pulse P(t) which for the purpose of that discussion had a zero rise time.

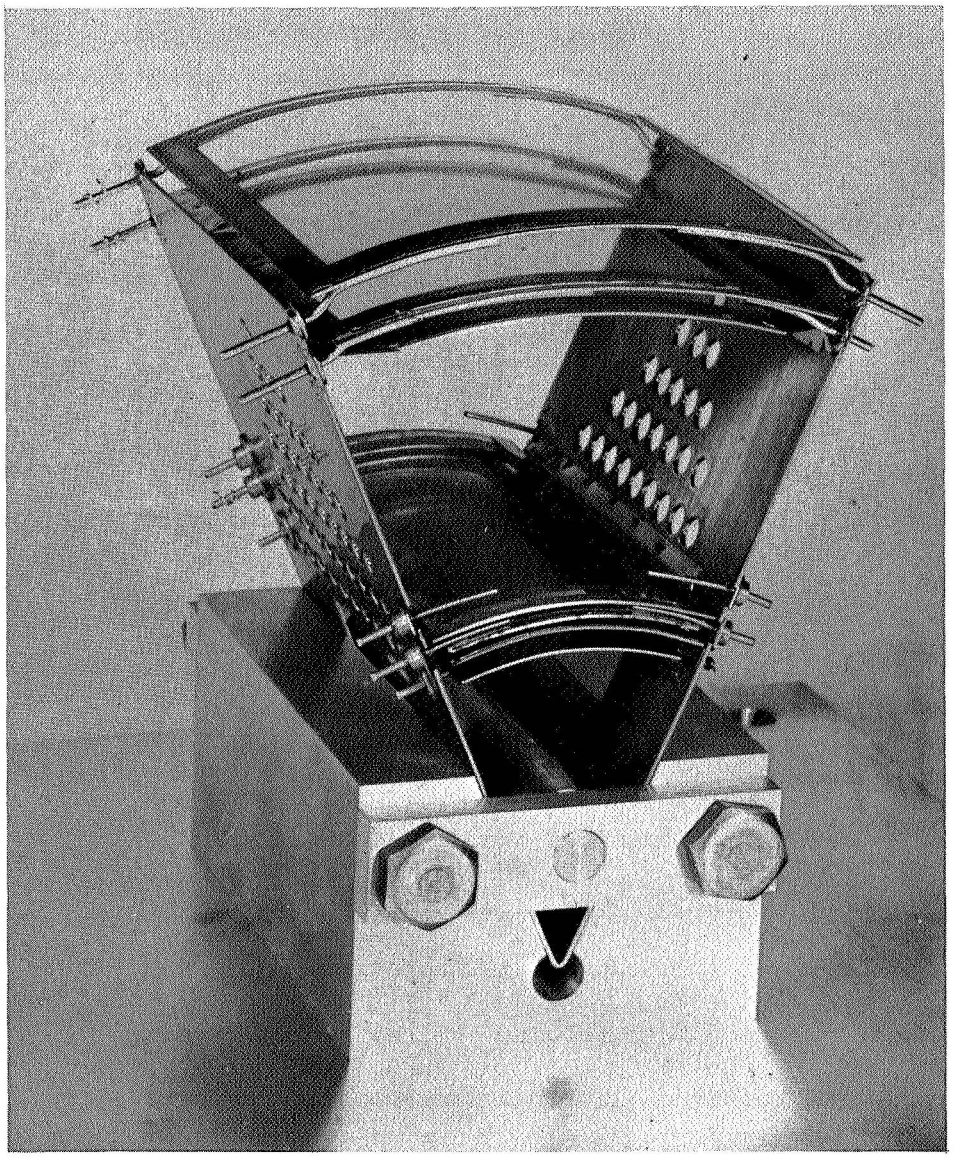

FIGURE 15. WEDGE TIME-OF-FLIGHT MASS SPECTROMETER WITH GRID STRUCTURE EXPOSED

Experimentally this is unattainable but the requirement of a fast rise time pulse is essential so that only a very small fraction of the ions leave the pulsing region before the pulse reaches maximum amplitude. The second requirement is that the width of the pulse be long enough for all the ions of interest to be accelerated out of the region. The third requirement is that the amplitude of the pulse be constant over the desired pulse width. The pulse repetition frequency is determined by the ion production and/or introduction mechanism, the pulsing region dimensions, and the flight time of the slowest ions. Ions can be produced in the pulsing region or introduced into it by some field or transport mechanism. The fall time of the pulse can be slow relative to the rise time since the constant amplitude width sets the highest mass number that can be quantitatively analyzed. Ions heavier than this maximum mass number may or may not be focused.

Since the maximum standard telemetry band has an upper frequency limit of 1050 Hz and the typical bandwidth required for this type of spectrometer is approximately 30 MHz, a wideband amplifier could not be used for the flight. To circumvent this problem a gated collector arrangement is employed. As has been mentioned, this arrangement consists of the three grids next to the collector in figure 15. With this gate, the telemetry frequency limit is not exceeded. The actual mechanism of the gate will be described in a following section.

Figure 16 is a block diagram of the electronics necessary for operating the spectrometer in a gated mode. If no gating were desired, the three grids of the gate structure could be removed. The circuitry associated with the gate, hence, would no longer be required. The electrometer would be removed and an electron multiplier substituted into the circuit. The output of the multiplier would then feed directly into a load resistor, the voltage across which would be placed into a wideband amplifier.

The circuitry associated with the pulse delivered to the source region (region 1) is straightforward. An astable multivibrator serves as a clock for the whole system. A monostable multivibrator is triggered by the main clock. This circuit sets the width of the ion accelerating pulse while the repetition frequency is controlled by the astable multivibrator. The monostable multivibrator output is amplified after which a dc bias is added. Normally, the dc bias 1 is equal to dc bias 2 if ions are being created in region 1. If ions are being introduced into region 1 then dc bias 1 is normally not equal to dc bias 2. The potential difference between dc bias 2 and dc bias 3 provides the necessary field for region 2.

Now let us consider the gate arrangement. The range of values for the repetition frequency of the clock is from 1 kHz to 100 kHz. This means that 1000 to 100,000 spectra are taken every second. Typical flight time values are 2.40 μs. for $^{30}NO^{+}$ and 2.65 μs. for $^{32}O^{+}_{2}$, so it is apparent that wide band equipment is necessary. However, as has been stated telemetry systems do not

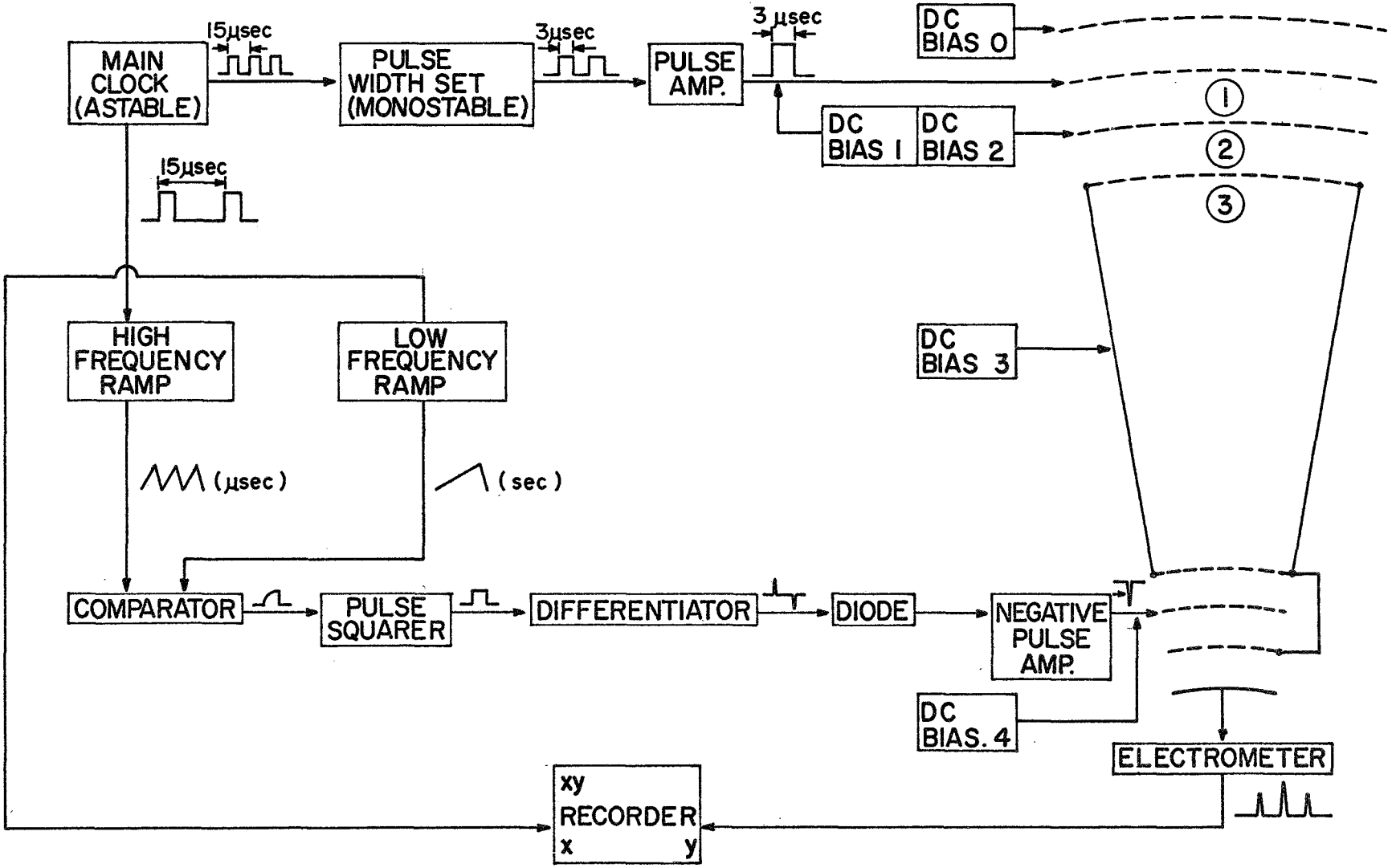

FIGURE 16. ELECTRONICS FOR GATED MASS SPECTROMETER

have an adequate bandwidth; hence, a gated system is required. The grid with the largest radius in the gate structure is used to terminate the field free region. The grid with the smallest radius is used to determinate the gate region so as to minimize the interaction between the gate and the collector. The middle grid of the gate structure is the gating component. On this grid is placed a dc potential that is just above the maximum potential an ion can fall through in the spectrometer. When this barrier is in place, no ions will reach the collector. If the barrier is lowered or removed for a short period of time, a burst of ions will be allowed to reach the collector if they have arrived at the gate region when the barrier is in its lowered state. From this one can see that if the time of the gate opening is swept relative to the beginning of the ion accelerating pulse, a spectrum can be obtained whose highest frequency components are determined by the rate at which the gate opening is swept. This assumes that the repetition frequency of the clock is sufficiently high that the integrated current seen by the electrometer produces a signal large enough to be discernable above the system noise. The electrometer is sufficiently slow in response that an integration can occur. The opening of the gate is accomplished by a pulse of short duration which has a polarity opposite to that of the barrier.

The electronics for obtaining and sweeping the gate pulse is also diagrammed in Figure 16. The main clock drives a high frequency ramp generator. A low frequency ramp generator running

independently of the main clock is compared against the high frequency ramp. Whenever the difference between the voltage levels of the ramps changes sign, a pulse is generated by the comparator. The pulse out of the comparator has its rise time enhanced by a second comparator. A derivative is then taken. The shorter the rise time, the sharper the pulses from the differentiator. The positive going "spike" is clipped. The negative going "spike" is then amplified and then impressed on dc bias 4. So, in essence, the sweeping of the gate pulse relative to the accelerating pulse is accomplished by the comparison of the time varying voltage states of the two ramp generators.

Finally, the ion current is detected by an electrometer which integrates the ion pulses. The frequency response of the electrometer must be chosen to be compatible with the low frequency sweep. Obviously, the faster the sweep, the more stringent the electrometer requirements.

Gating Systems

The introduction of a gating system is not a new instrumentation technique. Figure 17 shows two additional gating systems. The potentials are those for a positive ion measurement. The operation of these gates is similar in that the barrier is not removed but the ions arriving at the appropriate time are given additional energy enabling them to spill over the barrier. The gate shown in Figure 17 (b) is taken directly from Katzenstein and Friedland (1955). Both these gates were investigated

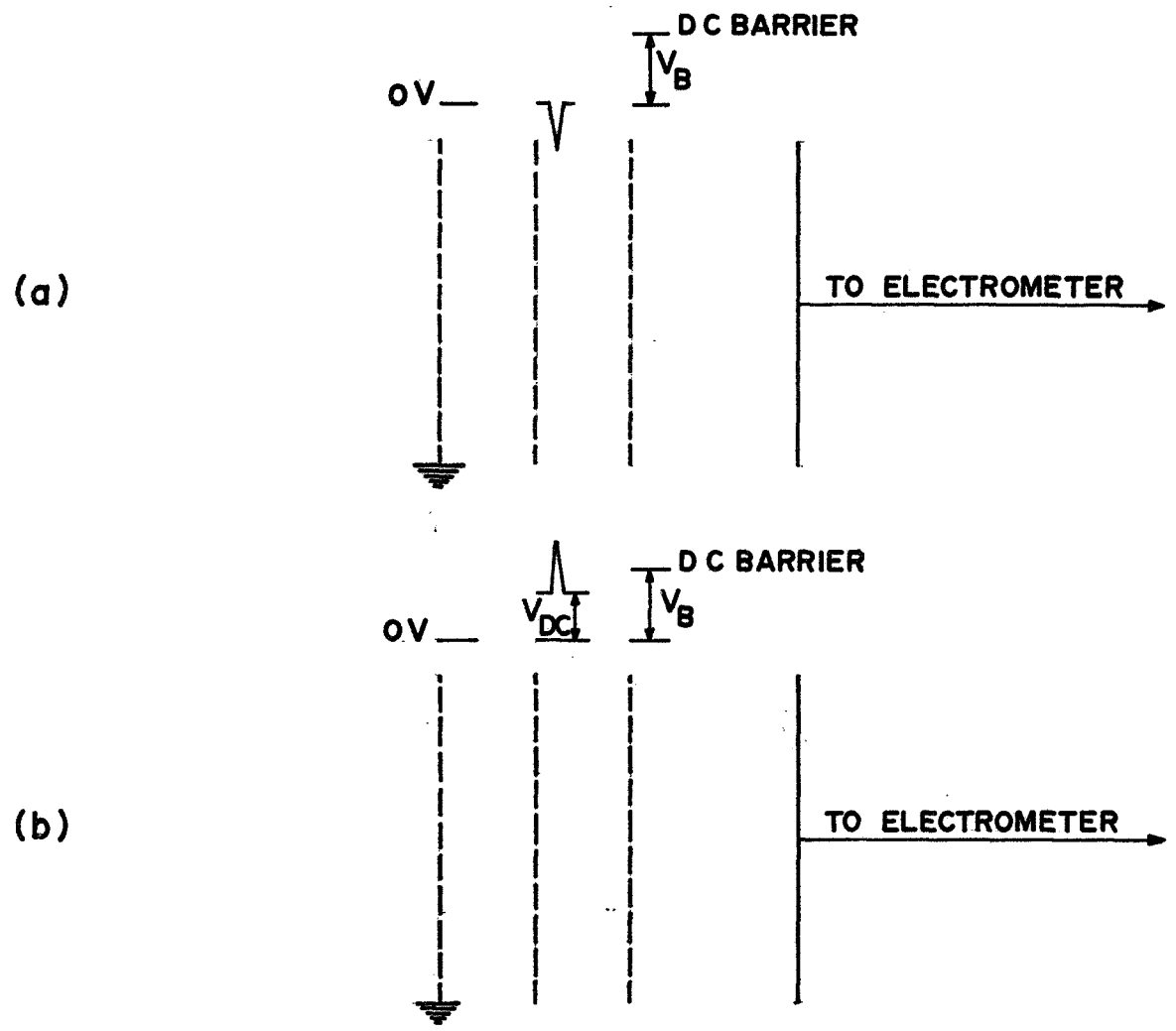

FIGURE 17. ALTERNATE GATE SYSTEMS

experimentally. Neither displayed any marked increase in instrument resolution and both displayed a slight decrease in sensitivity. The major disadvantage of these gates is that the collector is no longer shielded from the dc barrier. Two problems arise from this. The first is the possibility of a discharge to the collector which may damage the electrometer. The second is that any variation in the barrier potential within the frequency response of the electrometer will modulate the electrometer input. The first problem is not usually encountered in the lab but the possibility does exist during a rocket flight if certain malfunctions occur. The second is a problem in both the laboratory and flight because of the necessity of large voltage pulses which tend to unstablize the dc supplies.

Experimental Flight Time Determinations

Figure 18 shows the results of a survey of operating conditions. Here is plotted the log of flight time versus the log of mass. The voltage ratio is indicated by R and the potential on the first grid is given by V_1. The slopes of these straight lines should be 0.50; however, least squares fits give slopes of 0.46. It was originally thought that this deviation was due to fringing of the fields in the accelerating regions caused by the sides, top, and bottom of the wedge structure. The sides, top, and bottom are maintained at ground potential for constructional and electrical simplicity. When, however, an experiment was performed in which only the central portion of the accelerating region was used, the

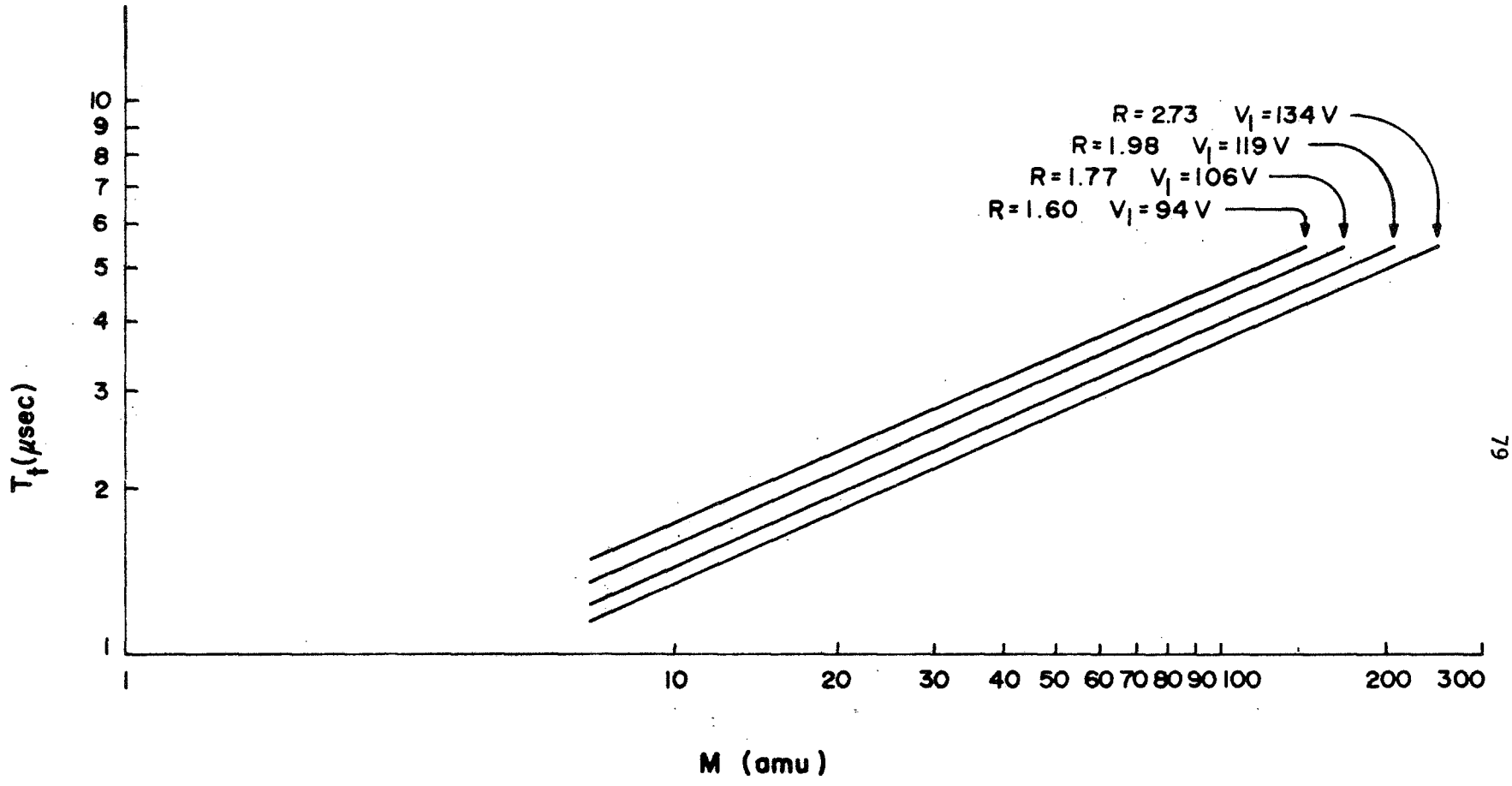

FIGURE 18. EXPERIMENTAL SURVEY OF FLIGHT TIMES FOR WEDGE SPECTROMETER

value of this slope increased only one percent. Upon closer inspection it was found that the ion source was the major cause of this discrepancy. The source that was used in these measurements was a surface ionization type. This source was similar in design to the one described by Kendall and Luther (1966) and identical to the one described by Diem (1967). The primary difference in this source from that of Kendall and Luther was that the emitting surface was an indirectly heated platinum button about 3 mm. in diameter. The use of this button allowed higher emission currents which relieved some of the signal to noise problems. However, having emission from such a large area increased the energy spread of the alkali metal ions that were emitted. In addition to this effect, emission from some surrounding areas forming the structure of the source was possible due to accidental deposition of alkali salts on these areas during the deposition of the salts on the platinum button. This would add to the energy spread of the ions emitted by the source. Also, it has been reported by Datz and Taylor (1956) that the emission of neutral alkali atoms is higher from platinum than for tungsten. This leads to the possibility of charge transfer reactions which are mass dependent. Heavier alkali metals have larger reaction cross sections than lighter ions (Hasted, 1964). Because of the design of this source, charge exchange for heavier ions can occur quicker and hence closer to the filament than for lighter ions. An energy analysis of the ions showed

that 10 percent of the ions had energies significantly less than the expected filament energy and this 10 percent had energies close to each other. By operating the spectrometer at low energy, two distinct peaks occurred for each of the expected alkali metal peaks. It should be remembered that operating at low spectrometer energy relative to the initial ion energy spread increases the effect of energy spread on the obtained spectra. The ^{23}Na peaks were approximately equal in magnitude while for ^{133}Cs the low energy peak was typically 30 percent lower in magnitude than the high energy peak, and at times, depending on filament temperature an order of magnitude difference between the ^{133}Cs peaks was observed. When the spectrometer was run at high energies, the two peaks would merge but the lighter masses would be more heavily weighted toward a longer flight time than the heavier masses which would cause a decrease in the slope of the lines that have been shown in Figure 18.

Data were taken with an electron bombardment source. This type of source ionizes gas atoms and molecules by collisions between the gas and electrons that have been accelerated to a terminal energy sufficient to detach electrons from the gas atoms and molecules. Typical slope values ranged from 0.48 to 0.52. Because this is a low resolving power spectrometer, further complications in interpreting spectra are introduced by the fragmentation of gas molecules.

Another possible source of error was the fluctuation in the starting and end points of the gate scan and nonlinearities introduced by the poor frequency response of the electrometer used in making these measurements.

Within the limitations introduced by the source and electronics, reasonable confidence can be placed in the root m dependence of time.

Comparison of Experimental Data with Theoretical Data

As has been seen, the best way to handle a large energy spread is to make the final energy of the ions much greater than their inherent spread. For this reason let us consider the flight times for R = 2.23. Table I lists a comparison of measured and predicted flight times.

TABLE I

COMPARISON OF PREDICTED AND MEASURED FLIGHT TIMES WITH GATED COLLECTOR

M (amu)	Predicted T_t (μ sec)	Measured T_t (μ sec)	Error (%)
23	1.72	1.96	+12.2
39,41	2.24	2.50	+10.4
133	4.30	4.36	+ 1.4

The percent error reflects the difficulties associated with the source. The ^{133}Cs is least affected by source difficulties and hence displays the best agreement between theory and experimental measurement. Figure 19 shows a spectrum obtained with R = 2.23.

Resolving Power

The resolving power of a time-of-flight mass spectrometer is given by

$$r.p. = \frac{M}{\Delta M} = \frac{t}{2\Delta t} \tag{111}$$

where t is the time at the maximum amplitude of the mass line and Δt is the width of the mass line at half maximum amplitude. The choice of the width at half height is arbitrary but is frequently used. The resolving power of the spectrometer operating with R = 2.23 as shown in Figure 19, is approximately 5. This low value of resolving power is partially due to the energy spread associated with the source. When this spectrometer is flown in the ionosphere, its resolving power should be higher since the ions observed will be essentially thermal. The theoretically maximum resolving power, i.e., no initial ion energy spread, with R = 2.23 is 17 assuming that Δt is width at the base of the peak because of the square nature of this line shape.

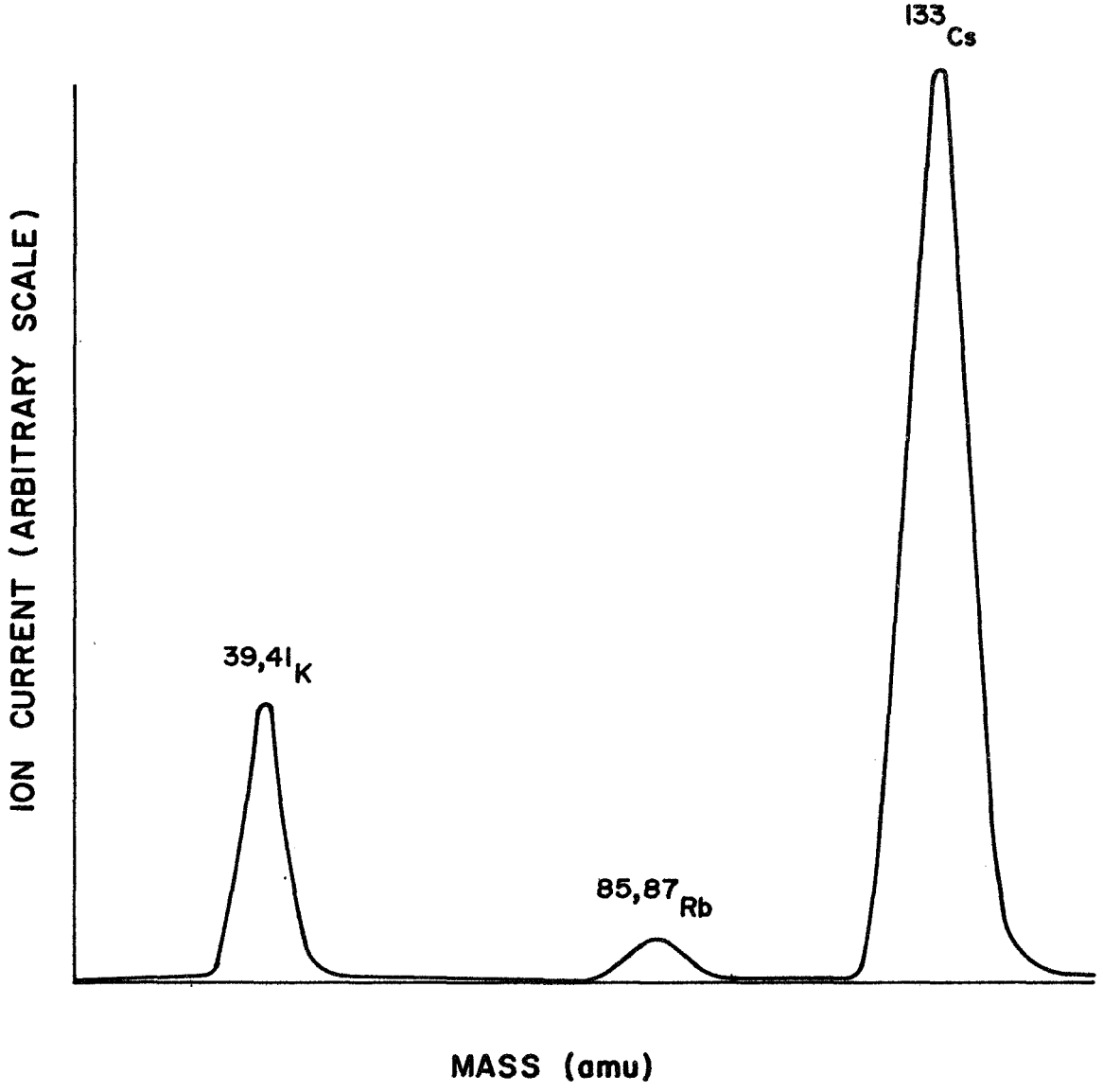

FIGURE 19. TYPICAL SPECTRUM FROM WEDGE SPECTROMETER

High Pressure Operation

One of the principal difficulties in making mass spectrometric measurements in the D-region of the ionosphere is the high ambient pressure. The experiments flown by Dr. Narcisi and Dr. Goldberg do not have the spectrometers operating at ambient pressure. On the contrary, the spectrometers are enclosed in vacuum chambers which are maintained at pressures several orders of magnitude below ambient. Ions are introduced into this chamber through a small orifice and then analyzed. There are several possible difficulties with this technique which shall be considered later.

Because of the relatively small flight path and large sampling or pulsing volume, the wedge spectrometer lends itself to reasonable operation at pressures encountered in the D-region. At 70 km the pressure is about 40 μ, at 80 km, 5 μ. Figure 20 shows the effect of pressure on sensitivity. This particular curve is for ^{23}Na in an air atmosphere. Air was used because the mean molecular weight in the D-region is approximately the same as at ground level. Several ion masses, e.g., $^{6,7}Li$, $^{39,41}K$, $^{85,87}Rb$, ^{133}Cs, were observed during this pressure performance testing with the higher mass sensitivity decreasing more rapidly than the lower mass sensitivity. This is expected since mean free path is a function of mass. Ions that participate in a collision are no longer focused, so that what is observed at high pressures is an increase in the dc current forming the baseline

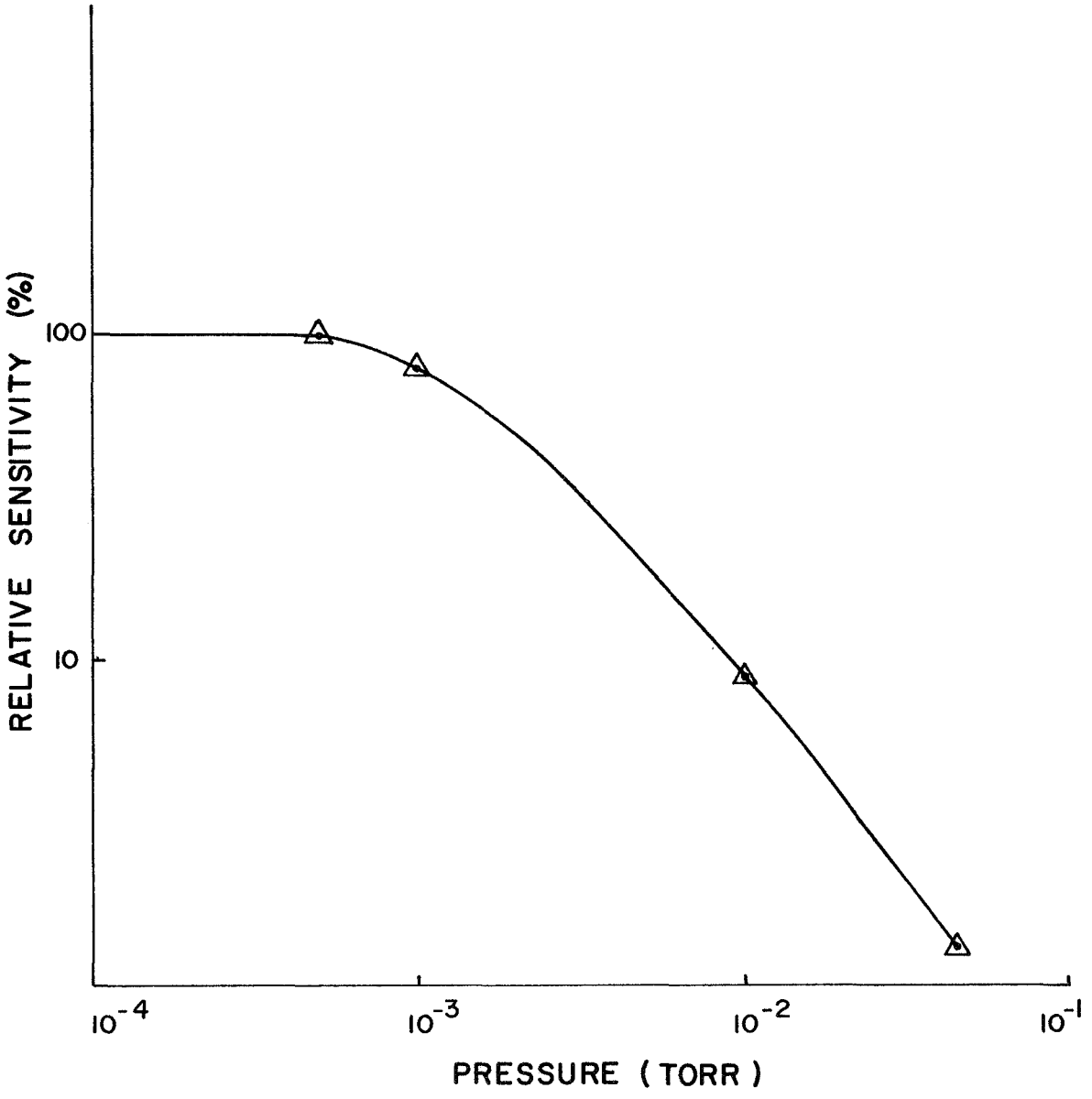

FIGURE 20. RELATIVE SENSITIVITY AS A FUNCTION OF PRESSURE FOR $^{23}Na^{+}$ IN AIR

of the spectra relative to the maximum current amplitudes of the peaks and a general decrease in current amplitudes of the peaks. No serious degradation in resolving power was observed up to 40 μ and useful spectra of $^{6,7}Li$ were obtained up to 60 μ.

The usefulness of this device at high pressures can be attributed, at least in part, to its high sensitivity. This high sensitivity is a result of the large volume of the pulsing region and is obtained at the expense of resolving power since energy focusing is enhanced by narrowing the pulsing region.

Mass Discrimination at Low Pressures

Since this spectrometer has been specifically developed to measure the ambient ionic composition of the ionosphere, ions are generally introduced rather than produced in the pulsing region. Unfortunately, in a collision free environment, the introduction of ions by means of attractive fields into the pulse region is mass dependent. The following simplified treatment will show in part how this dependence can occur.

Let us consider two planes of ions of the same mass which are separated by a small distance Δr_i. We will assume that all ions are at rest with respect to each other. The velocity of the rocket is given by v_R. Since the rocket is immersed in the plasma that constitutes the ionosphere, it is surrounded by a plasma sheath. The time for a plane of ions to traverse the sheath is from an energy consideration

$$T_\delta = \sqrt{\frac{m}{2q}} \int_0^\delta \frac{dr}{\sqrt{V(r) + \frac{mv_R^2}{2q}}} \tag{112}$$

where $\underline{m}$ is the mass of the ions, q is the charge of the ions, V(r) is the potential through the sheath relative to the plasma potential, and $\underline{\delta}$ is the sheath thickness. It will also be assumed that the potentials on the first and second grids of the pulsing region are equal. The total time that it takes for the first plane of ions to reach the second grid of the pulsing region is

$$T_1 = T_\delta + \frac{\mathcal{J}}{\sqrt{\frac{2qV_T}{m}}} \tag{113}$$

where $\mathcal{J}$ is the distance between the two grids, $V_T = V_R + V_B$ where V_R is the potential of the rocket relative to the plasma and V_B is the bias of the grids relative to the rocket.

For the second plane of ions, this same total time can be written

$$T_2 = T_\delta + \frac{\Delta r_i}{v_R} + \frac{\mathcal{J} - \Delta r_f}{\sqrt{\frac{2qV_T}{m}}} \tag{114}$$

where T_δ has already been defined, $\Delta r_i / V_R$ is the time for the plasma sheath to reach the second plane of ions, and $(\mathcal{J}-\Delta r_f) / \sqrt{2q\ V_T/m}$ is the time spent in the pulsing region with Δr_f equal to some distance not yet traversed by the second plane of ions. Since $T_1 = T_2$, then

$$T_\delta + \frac{\mathcal{J}}{\sqrt{\frac{2qV_T}{m}}} = T_\delta + \frac{\Delta r_i}{v_R} + \frac{\mathcal{J}}{\sqrt{\frac{2qV_T}{m}}} - \frac{\Delta r_f}{\sqrt{\frac{2qV_T}{m}}} \tag{115}$$

hence

$$\Delta r_f = \frac{\Delta r_i}{v_r} \sqrt{\frac{2qV_T}{m}} \tag{116}$$

From this analysis, it can be seen that the distance between the two planes is different in the pulsing region of the spectrometer than in the ambient plasma. This difference is directly related to the ion density difference between the ambient and the pulsing region. In general, the density will be reduced in the pulsing region relative to that of the ambient plasma. Unfortunately, it is also apparent that this reduction in ion density is mass dependent so that relative ion concentrations in the ambient plasma are not those measured by the spectrometer. As an example, if masses 1 and 16 were in equal concentration in

the plasma, the resulting spectra would indicate that the concentration of mass 16 was four times greater than mass 1. For the ions present in the D-region the discrimination would not be as great as that in this example; nevertheless, care would have to be exercised in interpreting the quantitative aspects of the spectra.

Mass Discrimination Associated with Gate Parameters

Ions of different mass that fall through the same potential will have different velocities; hence, the heavier ions will spend more time in the gate region than lighter ions. The gate should then be open long enough for the slowest ion of interest to pass through the gate. The maximum width of the gate pulse is constrained by the resolving power and sensitivity that is desired. For the operating conditions to be used in the rocket flight, the slowest ion would take approximately 78 nsec. to traverse the gate. These operating conditions will be considered in the section on the payload. Figure 21 shows an experimentally determined variation in current as a function of a change in barrier potential. By elevating the barrier potential ΔV above its optimum value while maintaining the accelerating and gating pulse constant, the time that the gate was opened is reduced. This time reduction occurs because the gate pulse is approximately triangular. From this curve, it is seen that a 20 V change from the optimum barrier potential produces a 76 percent decrease in the ^{133}Cs sensitivity while a 39 percent decrease in the $^{39,41}K$ sensitivity is observed.

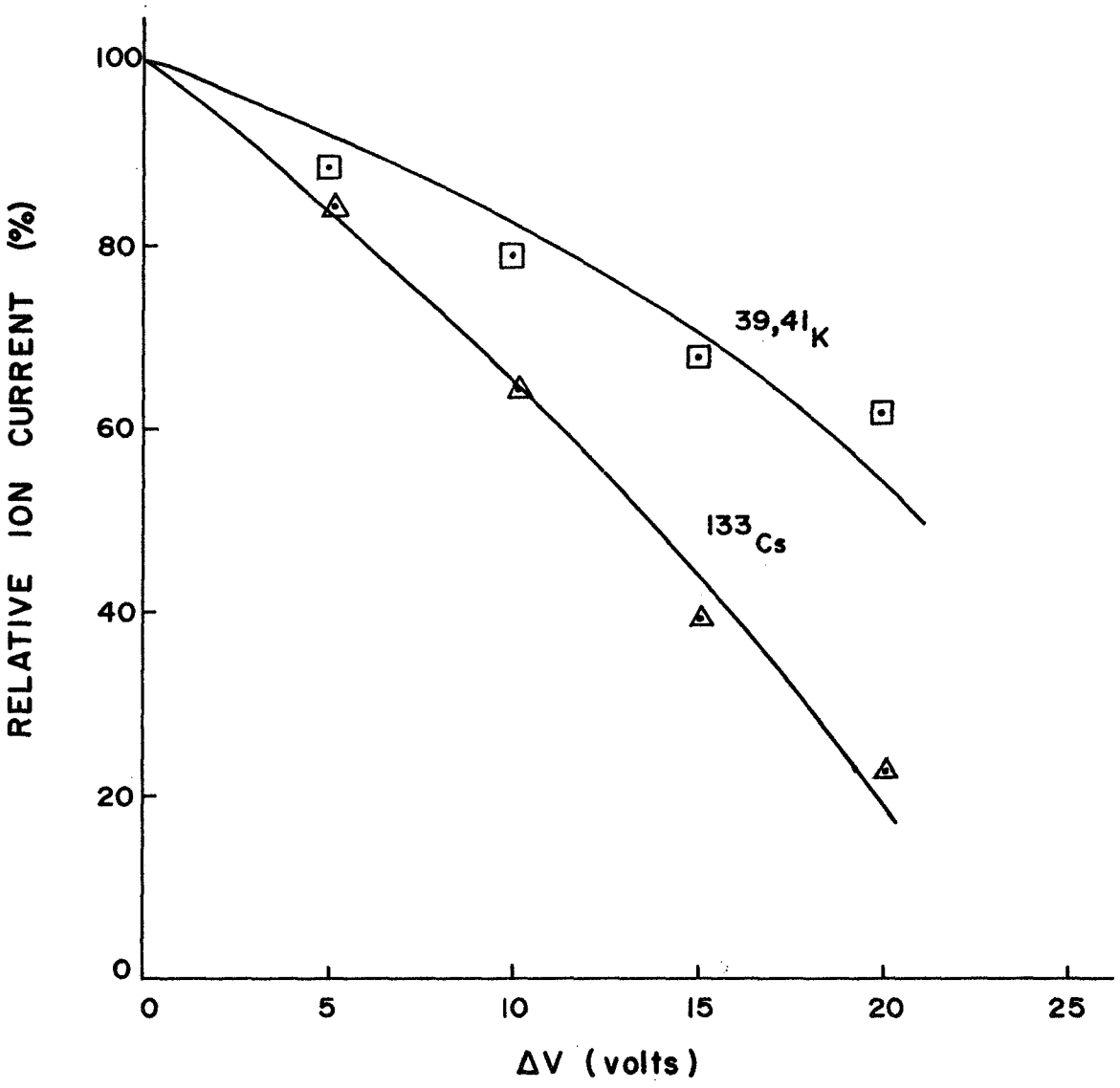

FIGURE 21. MASS DISCRIMINATION ASSOCIATED WITH GATE PARAMETERS

An exact analytical description of these curves depends on the exact shape of the gate pulse, the net usable volume of the pulsing region for the particular mass and the mass dependent energy spread of the source to make these measurements. However, it is obvious that care must be exercised in setting the gate parameters; otherwise poor quantitative results will be obtained.

Addition of Field Terminator Grid

When the pulse is applied to the first grid, field lines not only extend into the pulsing region, but also into the surrounding plasma. In order to set an upper limit on the distance that this field penetrates the plasma, an extra grid was placed in front of the pulsed grid of the spectrometer. Because of the short mean free paths associated with the D-region, no one doing D-region research has yet undertaken a detailed analysis of vehicle potential phenomena or of the plasma sheath associated with the vehicle or with the probe making measurements. Until such analyses are performed, the chemical influence of the vehicle and space probe on the ambient atmosphere will be a matter of conjecture.

The addition of this grid does not influence the operation of the spectrometer. When the pulse is off, ions drift in the region between this grid and the first grid because nearly identical dc potentials are maintained on both grids.

Estimate of Photoelectric Effect at the Collector

The maximum photocurrent density given by Bourdeau et al (1966) for a tungsten target at 120 km is 5×10^{-10} amp/cm^2. The area of the collector of the mass spectrometer is 9 cm^2. This would give an expected maximum photocurrent at the collector of 4.5×10^{-9} amp. If we correct for the transparency of the grids which is 85 percent, then for the seven grids of the spectrometer, the expected photocurrent would be 1.4×10^{-9} amp.

In order to get an experimental estimate on the photocurrent, two ultraviolet lamps were used to provide photons of wavelength comparable to those encountered in the D-region. The net flux and spectral distribution of one of the lamps was never thoroughly investigated; however, it was known that the minimum wavelength transmitted through its glass was 1800 Å. The second lamp that was used was designed, constructed, and calibrated by E.L. Gee (1966). The measured photon flux at 30 cm. from the window of this lamp was 2.6×10^{11} photons/sec-cm^2 and predominately Lyman α at 1215.7 Å. According to Bourdeau et al (1966), the expected solar radiation of Lyman α is 2.7×10^{11} photons/sec-cm^2.

An experiment was performed in which the uncalibrated UV lamp was shone directly on the collector. The current was between 5×10^{-14}a. and 1×10^{-13}a. which was comparable to the noise of the system. When the calibrated lamp was shone directly at the collector, a photoelectric current of less than 1×10^{-11}a. was

observed. However, if a spherical wavefront is assumed, the photon flux at the collector should have been approximately a factor of 36 greater than the photon flux of the solar radiation. This experiment was performed with many variations in the angle of the lamp relative to the normal of the collector, at various pressures from 1×10^{-6} torr to 2×10^{-1} torr with air, NO, acetone and benzene atmospheres. The lamp itself was tuned over its band of operating conditions and care was taken to maintain a reasonably pure H_2 atmosphere in the lamp. From the forgoing can be drawn three possible conclusions. The first is that the lamp calibration left something to be desired. The second is that the photon flux in the D and E region is incompletely known. The third is that the stainless steel used in the collector has a poor electron per photon yield.

In order to cope with the possibility that a current in the 10^{-9} a range may occur, it is suggested that the rocket be launched near sunset and away from the sun. It may also be stated that the photocurrent may yield information about payload orientation. Finally, it is obvious that night measurements are not as likely to be troubled by photoelectric effects.

Discharge Investigation

Since there are pulses used in this spectrometer that are 80 V in magnitude, some concern can be expressed about the possibility of striking and sustaining a discharge. Although no

absolute test could be arranged, some meaningful tests were performed to check for discharging. The regions of the spectrometer where the pulses are applied were immersed in electrons and ions without any discharge resulting. Electrons were accelerated to over 200eV in these regions up to pressures of 200 μ. Simultaneously with electron bombardment and separately, ion beams in the 10^{-7} a range were impinged on the pulsing regions. No discharges were visible and no anomalous effects or failures were observed in the electronics. The electronics used in this test did not incorporate current limits as do those in the payload and hence were more susceptible to damage.

Electron Multiplier Detector

A method for enhancing the sensitivity of the mass spectrometer is the addition of an electron multiplier to the detection circuit. A 19-stage venetial blind multiplier was attached behind the collector which had a hole cut in it at the same level on the ion to electron conversion dynode of the multiplier. The flight path of the spectrometer in this experiment was 6.0 cm. Figure 22 shows a spectrum that was obtained with this arrangement. This particular spectrum was obtained by J. Rarick and E.E. Barnes.

This excellent agreement can be attributed to a dc retarding potential applied to the first grid of the spectrometer which prohibited low energy ions from entering the pulsing region, and to the stability and linearity of the electronics that were used.

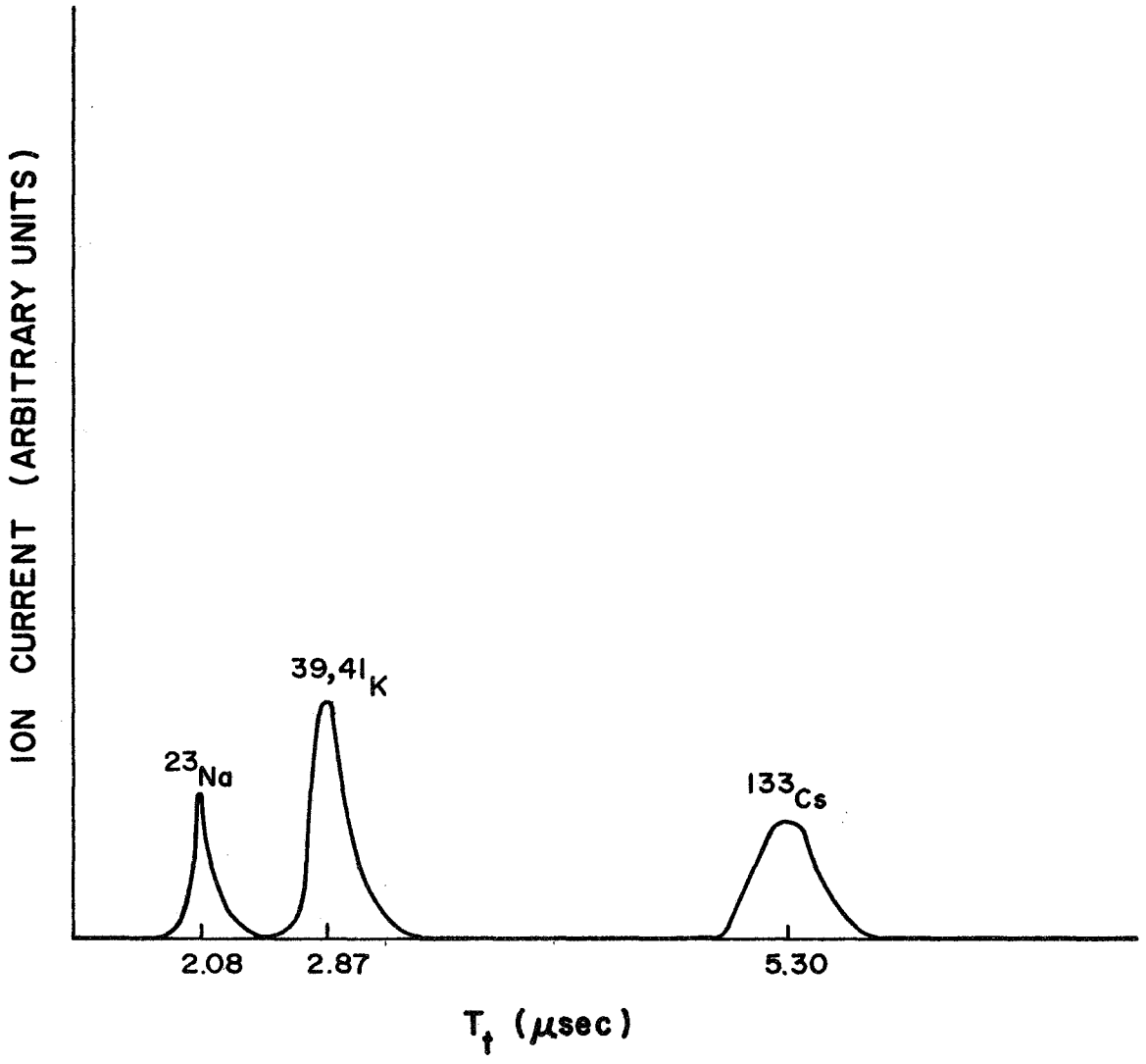

FIGURE 22. SPECTRUM TAKEN WITH WEDGE SPECTROMETER WITH ELECTRON MULTIPLIER DETECTOR

Table II lists the computer-predicted flight times and the measured flight times.

TABLE II

COMPARISON OF PREDICTED AND MEASURED FLIGHT TIMES WITH GATED COLLECTOR

M (amu)	Predicted T_t (μ sec)	Measured T_t (μ sec)	Error (%)
23	2.16	2.08	3.7
39,41	2.81	2.87	2.1
133	5.23	5.30	1.3

The primary problem that has to be investigated before such a device is attached to a flyable mass spectrometer is the behavior of the multiplier at high pressures, namely, those encountered in the D-region. The voltage applied across the multiplier was 3 kv which would most likely cause a discharge at these pressures; thus low voltage operation should be considered and balanced against loss of gain in the multiplier

IV. PAYLOAD DESCRIPTION

Mechanical Considerations

Vehicles

Three mechanical designs were prepared because three different programs, each with different vehicles, were under consideration. The first configuration of the payload was for a Nike-Tomahawk vehicle. The experiments on this vehicle were to be a quadrupole mass spectrometer of Dr. Goldberg of NASA Goddard, Greenbelt, Maryland, and the time-of-flight spectrometer that has been described. The primary motivation behind the experiment was to compare the data and draw conclusions concerning any possible discrepancies in the data. This would definitely enable a comparison of the two different sampling systems of these spectrometers. Because of several misfortunes encountered during this joint venture, the program was suspended until 1970 or 1971. The second configuration of the payload was developed for a Sidewinder-Arcas HV vehicle. This was a program with Mr. Ballard at White Sands Missile Range, White Sands, New Mexico. A completed payload was taken to this range and tested but was not launched due to a incompatibility in telemetry transmitting and receiving. The third configuration is for a Boosted Arcas II vehicle. This configuration is almost identical with the Sidewinder version with the exception of the rocket skin of the payload region. The Sidewinder version had an aluminum skin which necessitated a twin antenna system. An antenna was mounted on the rocket skin and

driven by the payload antenna. It is necessary for the telemetry carrier to be on at all times during the flight so that the directional antenna of the receiving station can remain fixed on the payload position. In the Boosted Arcas II version, a fiberglas rocket skin is used which enables the payload antenna to supply the carrier for the receiver. The following sections will describe the second and third configurations.

Sealed Electronics Structure

The electronics section of the payload was designed in such a fashion as to be pressure tight, i.e., leakage of gas from the electronics structure was undesirable. It was undesirable for two reasons. First, the gas that would escape from this structure would introduce contaminants which could be ionized and then sampled by the spectrometer; thus, the data would not reflect true ambient constituents. Secondly, the reduction of pressure in the electronics section would remove convective dissipation of heat from the components which in turn could cause component failure.

Vacuum Chamber for Pre-Flight Testing

A vacuum chamber made of stainless steel was incorporated into the payload to facilitate pre-flight testing. This chamber had mounted in it a surface ionization ion source. This source was designed to sustain the rigors of the flight even though it would not be used during the flight. However, the safest procedure would be to remove it before the flight and replace it with a simple

stainless steel cap. If during lift off or payload separation, vibration or shock caused parts of this source to become free, there is the possibility that these parts could damage the spectrometer. The disadvantage of adding a plug after testing is that vacuum would have to be broken.

After testing is completed the pressure in the vacuum chamber should be elevated to a pressure above that of the altitude at which payload separation occurs. The safest procedure would be elevating the pressure to about 10 mm of Hg to account for possible early payload separation or to just below atmospheric pressure. The first of these is chemically slightly preferable. The gas used in elevating this pressure should be dry nitrogen since the primary atmospheric neutral constituent up to 80 km is nitrogen. Since expected ionic species are protonated water clusters (Narcisi, 1967), water vapor should be excluded.

The vacuum chamber should be baked in order to reduce contamination. The maximum temperature during the bake is set by the temperature acquired by the electronics structure. Provision is made to monitor temperature within the electronics structure close to the vacuum chamber. Figure 23 is a photograph of the external mechanical structure of the payload.

Separation of Payload From Vehicle

The payload is separated from the vehicle by an explosive charge that is placed at the base of the payload. When the charge is detonated, the payload slides up the rocket skin and leaves the

FIGURE 23. EXTERNAL MECHANICAL COMPONENTS OF EXPERIMENT PACKAGE

vehicle completely. This action can be looked upon as similar to the standard military mortor where in this case the payload is the mortor projectile and the rocket skin is the mortar tube. Atlantic Research Corporation recommended a design criterion of 90g although measured shocks were 66.4g and a time to peak of 0.005 seconds. It should be stated here that other information less stringent was also obtained from other sources. The payload underwent a simulated separation shock test on a vibration table at NASA Goddard. Also, an actual separation test using the explosive charge present during flight was performed at Atlantic Research Corporation. The payload successfully met both of these tests.

Shake Testing

The payload has successfully undergone shake testing. This package has passed tests which qualify it for flight on both the Arcas and Nike-Tomahawk vehicles. The Nike-Tomahawk is considered to have one of the most violent vibrational profiles relative to other sounding rockets.

During this testing, some holes were accidently punched through the grids in the accelerating regions by NASA personnel, i.e., the holes were not the result of shaking. These holes were as large as a half an inch in diameter. The spectrometer with these holes still functioned with small or no loss in resolving power.

Separation of Nose Cone and Vacuum Chamber From the Payload

At an altitude of about 70 km, the payload will be expelled from the vehicle. When the payload has approximately a third of its length protruding above the top of the skin, a ball-lock arrangement is released. The release of this locking arrangement allows a compressed spring to expand. This spring is attached to the nose cone and also the vacuum chamber. When the spring is fully expanded, the nose cone and vacuum chamber will have a separation velocity of approximately 21 ft/sec relative to the payload. If a malfunction in the timing fuse of the separation charge produced an early payload separation drag forces could reduce this separation velocity. If we assume that the vehicle was traveling at Mach 3, which is in fact approximately the expected velocity, the retarding force on the cone will be 2.7* lbs. at 50 km.

During the removal of the vacuum chamber, it was feared that the sides of the chamber would collide with the spectrometer. A photographic study and fifteen test firings allayed this fear.

Payload Weight and Center of Gravity

In order to predict the altitude attained by the payload, its weight and center of gravity had to be determined. The payload weight of the Sidewinder version was 17 lbs. while the Boosted Arcas II version was 16 lbs. The difference resides in the lighter fiberglas

*Value based on data obtained from NACA tables.

skin of the latter. The center of gravity for the Boosted Arcas II version which was launched was 13.15 ± 0.005 inches from where the base of the payload meets with the rocket motor.

Electronics Considerations

Determination of Repetition Frequency and Electrometer Requirements

The volume of the pulsing region is 17.15 cm^3. In order to fill the volume completely at the slowest speed, which is near apogee and which for the vehicles considered is about 350 m/sec, 14.3 μ sec is required. It is desirable to analyze masses that are quite heavy since D-region measurements made to date have not analyzed species above a hundred atmoic mass units. Consequently, a pulse width of 3.00 μ sec was chosen which would insure proper operation up to mass 250. With this pulse width, reasonable high mass performance could be expected even if the pulse height decreased. In order to determine the period of the pulses, the fill time and pulse time were summed yielding 17.3 μ sec.; and, hence, the repetition frequency is 57.8 KC. As is obvious, ram filling has been assumed and the effects of the vehicle potential and bias on the field terminator grid have been neglected.

When the pulsing region is allowed to fill completely between pulses, an estimated total ion concentration can be made. If, however, the spectrometer is flown in conjunction with some other total ionization monitor, then the repetition frequency can be

increased so as to increase sensitivity at lower altitudes where the fill time is less. A reasonable increase in the repetition frequency will increase the net current seen by the collector. However, the period between pulses cannot be less than the flight time of the heaviest ion since this would cause the peaks from different individual spectra to overlap.

If it is assumed that the concentration of NO^+ at 75 km is $300/cm^3$, then the net charge in the pulsing region 8.24×10^{-16} coul. This assumption of the ion concentration is based on Narcisi's (1965) results. If we assume that this charge arrived during the 17.3 μ sec of the pulse period, then expected current would be 4.76×10^{-11}a. Correcting for the 85% transparency of the grids of the spectrometer reduces the current to 1.53×10^{-11}a. If we assume that the vehicle is traveling at Mach 1.5 at 75 km and a normal shock* exists in front of the spectrometer, then the pressure in the spectrometer is about a factor of 2.5 greater than the ambient pressure which is about 20 μ. Thus, the spectrometer operating pressure is about 50 μ. Using the experimental data on the relation between sensitivity and pressure, the ion current should be reduced by about a factor of 75. Then, the expected current is about 6.4×10^{-13}a.

The assumption of a normal shock existing in front of the spectrometer cannot be rigorously justified but has been made to give a crude approximation of the expected current. This assumption is

*A normal shock exists when the flow vector does not change direction on passage through the shock front.

the worst that can be made and actual instrument performance should probably be better.

On the basis of these calculations, the minimum detectable current should be set at 1×10^{-13}a which would give about 50 ions/cm^3 sensitivity at 75 km. At 90 km where pressure corrections do not have to be made 1×10^{-13}a, would give a particle sensitivity of about 2 ions/cm^3.

These calculations also assume that the spectrometer normal vector and the velocity vector are parallel and, as already mentioned, ram filling of the accelerating region is the predominant filling mechanism. If the angle between the spectrometer normal and the velocity vector becomes large, then ram filling is no longer the predominant mechanism. The potential gradient between the pulse terminating grid and the plasma becomes the primary mechanism for filling. This potential gradient is a function of payload potential relative to the plasma which in turn is a function of altitude.

In order to treat this sensitivity problem completely, an analysis similar to that of Sonin's (1966) considering the geometry of R. Narcisi's experiment is required.

Vehicle Potential

If a body is placed in a neutral plasma, it will take on a negative voltage with respect to the plasma because more electrons will collide with the body than ions. If the electrons are at the same temperature as the ions, the electrons will be traveling the square root of the ratio of the ion mass to the electron mass faster

than the ions. In the D-region, the electron temperature is slightly greater than the ion temperature (Biondi, 1968) which would tend to drive the body slightly more negative. A competing effect which tends to drive the vehicle positive is photoemission during a daytime launch, which is intended. Another influencing factor on vehicle potential may be the total spectrometer ion current but this is approximately two orders of magnitude below that of an unretarded photocurrent from the payload skin of 10^{-6}a based the value of 5×10^{-10} amp/cm^2 given by Bourdeau et al (1966). Based on the data presented by Willis (1965) and obtained from conversations with Narcisi (1967, 1968), the vehicle potential even with photoemission should be negative since the ratio of the payload skin area to the sampling area is about 37. Thus, a good return path is established between the spectrometer and the plasma.

Potential on the Pulse Terminator Grid

The dc potential on this grid, which will be called the zeroth grid because it is not essential for spectrometer operation, is set to -10 V relative to payload skin. This may not be a very desirable potential from a chemical viewpoint because ions accelerated through a potential of this magnitude can possibly participate in reactions or excitations which could modify the ambient atmosphere being sampled. If the payload swings negative then -10 V is the minimum potential difference between this grid and the plasma. On a future payload, it would be desirable to sweep this potential to check on the possibility of chemical reactions induced by this potential.

But, this first payload is oriented more toward system trial and evaluation.

Potentials on the Pulsed Grid and Second Grid

The dc potential of the pulsed grid, which will be called the first grid, will be set to -5 V relative to the payload skin or chassis. This potential will act as a retarding barrier which will lessen the probability of chemical events occurring in the region between the zeroth and first grid. The second grid of the spectrometer will be set to payload chassis potential.

In the laboratory, the overall performance of the spectrometer is governed by the energy spread associated with the particular ion source that is used. This spread necessitates larger accelerated pulses than is required for best space focusing. In the ionosphere, one has the near perfect ion source. The ion temperature is just slightly above the neutral gas temperature of about 225°K (Biondi, 1968). Consequently, the accelerating pulse voltage can more closely approach the conditions for best space focusing. The best space focusing pulse height was about 45 V. However, because some energy spread will be introduced during the filling of the region, a pulse height of 75 V is desirable to offset the spread. This spread could be reduced by raising the dc potential of the first grid to -1 V, thus setting the maximum spread to less than a volt; however, if for some reason the payload skin would swing positive more than one volt relative to the plasma, the ion current into the pulsing region would be cut off, so the -5 V was chosen on a prototype criterion.

Remaining DC Potentials and Gate Pulse Height and Width

The potential of the third grid is minus 60 V with respect to the payload chassis. The fourth grid which is the beginning of the gate region is common to the third which is also common to the sides, top and bottom of the wedge. The gate dc potential is set to + 70 V dc since the accelerating pulse of 75 V is applied to a -5 V dc level, so the net voltage is 70 V relative to payload chassis. The width of the gate pulse at the base is 90 to 100 nsec. and its height is about -80 V. Mass 150 takes approximately 78 nsec. to traverse the gate. Thus, quantitative measurements can be made at least up this mass if all necessary calibrations are made. The grid terminating the gate region is common with the sides of the wedge and thus is at -60 V relative to payload chassis. Finally, the collector is held at -60 V.

Sweep Conditions and Electrometer Frequency Response

The gate is swept from 0.3 μ sec. to 6.0 μ sec. which sweeps over the range from mass 1 to 250. This scan occurs over a two second interval which gives adequate altitude resolution for the data obtained. With this scan rate, a frequency response of 1000 Hz at 10^{-11}a is adequate to insure that RC smearing will not be excessive.

Spectrometer Shield

In order to prevent the exposing of the sides, top, and bottom of the spectrometer to the plasma, a shield is placed around the spectrometer similar in application to that of a guard. This shield is held at 0 V relative to the experiment package chassis.

Summary of Requirements

A summary of the electronic requirements for the spectrometer is listed in Table III.

Block Diagram of Payload Electronics

Figure 24 is a block diagram of the electronics of the payload. The section of this diagram pertaining to the accelerating and gate pulses is identical to that described earlier and will not be discussed here. The diagram of the dc control describes the dc distribution to the grids and is self explanatory on the basis of the previous section. The dc power supply for the whole payload was designed and built by Betco Electronics, Burtonsville, Maryland.

In addition to the primary functions required for spectrometer operation, several pertinent additions have been made to the electronics. The first of these is the addition of time markers. By time markers are meant that when the gate pulse is at 1 μ sec. and 3 μ sec. relative to the leading edge of the accelerating pulse, narrow square pulses are generated and fed into the lower frequency channel of the telemetry, which will be discussed later. These two time marks help define the mass scale. The operation of this circuit addition is straight forward. The leading edge of the varying width pulse coming from the pulse width modulator triggers both the 1 μ sec. and the 3 μ sec. monostable multivibrator. The trailing edge of this pulse is fed into the gates. If the trailing edge of the pulse occurs at the same instant as or after the trailing edge of one of

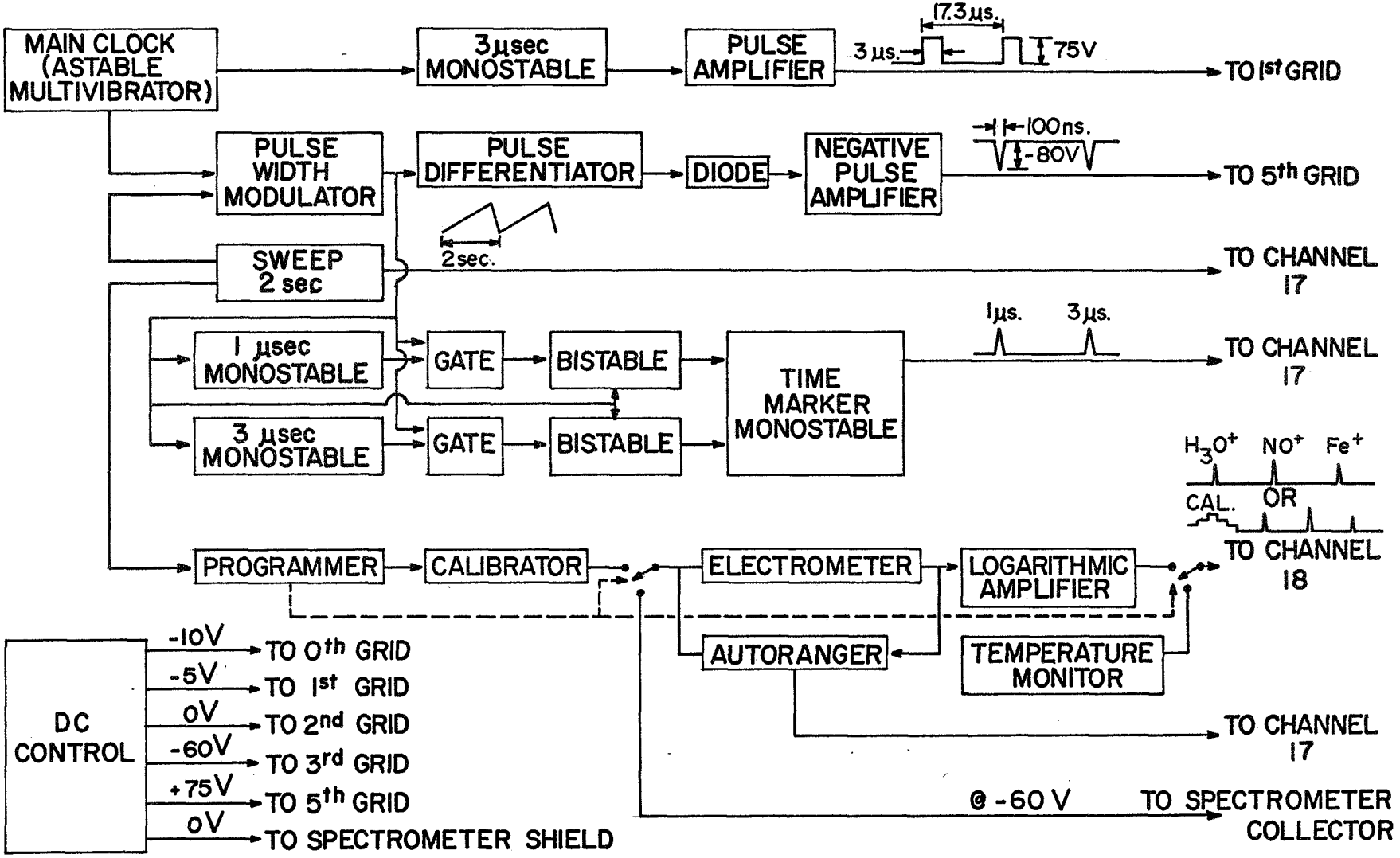

FIGURE 24. BLOCK DIAGRAM OF THE ELECTRONICS FOR THE WEDGE SPECTROMETER PAYLOAD

the monostable pulses, the appropriate gate triggers a bistable multivibrator. This bistable multivibrator in turn triggers a monostable generating the time marker. The bistables are reset by the fly back of the slow sweep circuit.

The slow sweep circuit also triggers a small computer, which is designated as programmer in the block diagram. This computer interrupts the beginning of every third slow sweep or spectrum. Its first function is to place on the high frequency, channel 18, a voltage which is related to the temperature of the electrometer and log amplifier area of the payload. Next, it sequences through three calibrating currents which determine the relationship between the log amplifier voltage output and the collector current.

Finally, the last addition is the autoranger which is a logic circuit that determines which of the two feedback resistors are used in the electrometer. Whenever the spectrometer collector current exceeds a certain level, this circuit will decrease the sensitivity of the electrometer. Similarly, if the collector current drops below a minimum level in this less sensitive range, this circuit will increase the sensitivity of the electrometer. Whenever a change in range occurs, a pulse is placed on channel 17 by the autoranger. Because of volume constraints and the necessary dynamic range required of the electrometer, a two range system is used with a logarithmic amplifier which, however, makes data reduction more tedious. On future payloads on larger vehicles, a six range linear system would be highly desirable.

A detailed description of all the circuitry that has been discussed will appear in the thesis of E.E. Barnes.

Telemetry

The carrier frequency for the telemetry is 1680 MHz. This frequency was chosen because it is the standard frequency of the weather payloads that are launched on balloons and rockets. The total system was an FM/FM system. In this system, the analog signals drive voltage control oscillators (VCO's) which in turn are used to frequency modulate the carrier. The two subcarriers frequencies were 70 KHz, which is IRIG* channel 18, and 52.5 KHz, which is IRIG channel 17. The frequency response of channel 18 is 1050 Hz and the frequency response of channel 17 is 790 Hz. From this it is seen that the 1 KHz frequency response of the electrometer was close to the limit of the capability of the telemetry system.

The standard receiving system for this carrier is the GMD** system. However, the GMD is not as a rule equipped for FM/FM decoding but AM/FM. Consequently, in order to use the GMD, the signal must be tapped from the IF*** which can then be further processed back into analog data by discriminators at the appropriate subcarrier frequencies.

The VCO's, mixer, and transmitter were designed and built by Betco Electronics, Burtonsville, Maryland.

*IRIG: Interrange Instrumentation Group
**GMD: Ground Meteorological Detection
***IF: Intermediate Frequency

The antenna used for transmitting was a modified circular slot originally described by Cuffin (1965). Cuffin also studied the pattern of this modified antenna and found one node. Information on payload spin can be obtained from the presence of this node. This antenna has been successfully used by Hale (1967). Figure 25 and 26 are photographs of the electronics structure.

Electronics Test of the Experiment Package

All circuits were individually tested and the system as a unit was tested. By this is meant that all the appropriate dc voltages and pulses were applied to the spectrometer. In addition, the telemetry and antenna system were checked and shown to be operational. Analog data consisting of the electrometer, calibration, temperature monitor, slow ramp, range change marks, and time marks were obtained using the telemetry and antenna system. Finally, the surface ionization source was turned on at a high pressure and an ion burst from the source was measured by the spectrometer. This measurement again was made with the telemetry link.

Launching of Rocket

On October 29, 1969, the first of the two constructed packages was launched from Wallops Island, Virginia. The flight was designated as NASA Arcas 15.42. Launch occurred at 1605 EST. The vehicle was tracked by Wallops Island radar and telemetry transmission was received by the Wallops Island Weather Station and the Ballistic Research Laboratory telemetry van. The first and second stages of

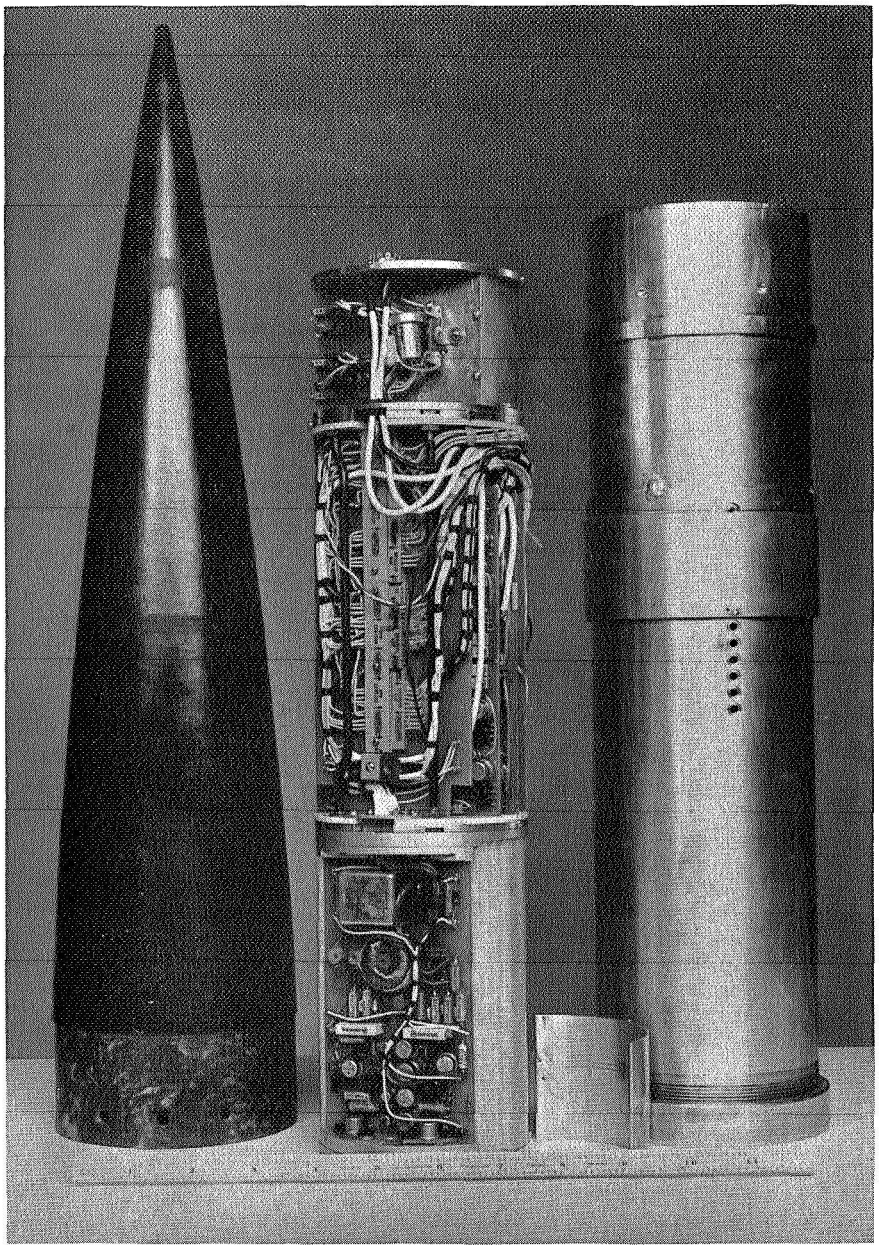

FIGURE 25. ASSEMBLED ELECTRONICS STRUCTURE WITH NOSE CONE AND VACUUM TIGHT SKIN

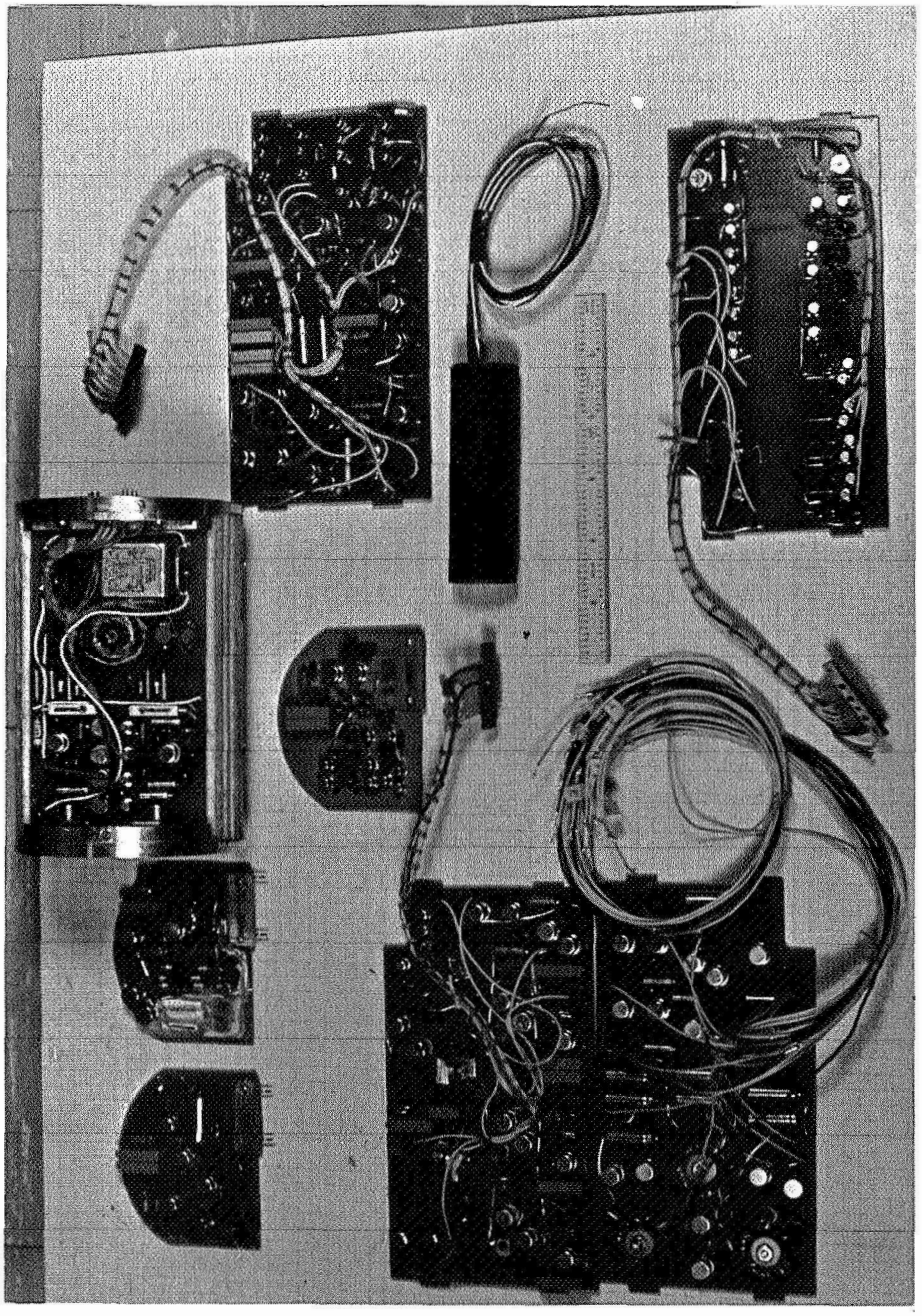

FIGURE 26. PRINTED CIRCUIT BOARDS WITH POWER SUPPLY AND TELEMETRY

the rocket performed excellently. However, payload separation never occurred because the explosive charge was not present in the second stage. Due to an error on NASA's part, the wrong second stage motor was used. Because separation did not occur, the spectrometer was never exposed to the ionosphere; hence, no spectra were obtained.

On the brighter side, this flight provided proof that most of the electronics can function well throughout a flight. Telemetry records of the temperature in the electrometer region, electrometer calibrations, mass scan, time marks, and range change marks during electrometer calibration were obtained.

V. SUMMARY AND CONCLUSIONS

A cylindrical time-of-flight mass spectrometer with a double accelerating region has been analyzed theoretically. A computer program has been developed to predict the flight times for ions in this spectrometer. This has allowed a detailed study of the space focusing properties of this instrument. It has been shown that the space focusing properties of this instrument are superior to that of a comparable linear device. A spherical time-of-flight mass spectrometer with a double accelerating region has also been theoretically analyzed and computer program has been written to yield flight times necessary for the study of space focusing. This analysis has indicated that this spectrometer has superior space focusing relative to cylindrical and linear devices of the same dimensions.

A cylindrical wedge mass spectrometer has been experimentally investigated. This instrument is similar enough to the full cylinder instrument that the flight times predicted by the full cylinder theory are reasonably close to those experimentally observed. This wedge spectrometer has displayed a resolving power of 5 within the constraints of the ion sources that have been used. Because of its short flight path and high sensitivity it has been able to operate at pressures up to 60 μ. An electron multiplier was added to the detector circuit in place of a gated collector detection method. An increase in the flight path from 4.4 cm. to 6.0 cm. increased the resolving power to 7 with the multiplier as the detector.

It is suggested that an experimental investigation of the full cylinder and the spherical mass spectrometers be conducted. Because of their inherent high sensitivity, they could be used as partial pressure analyzers and for studying chemical reaction kinetics at reasonably high pressures. The use of the orbitron principle as a method of producing ionization in the pulsing region has been a topic of discussion among Dr. Kendall, this author and co-workers. A study of the ability to obtain quasi-circular electron orbits between the first two grids while being compatible with the spectrometer operating conditions would be required. It is also suggested that an investigation of the operation of electron multipliers at high pressures and low voltage be considered.

A complete instrument package has been developed for use in the D-region of the ionosphere. This payload has been designed for flight on a small vehicle but could be adapted for use on a large rocket. The wedge spectrometer has itself been tested and successfully withstood the vibrations associated with a large vehicle. The capability of being flown on a small rocket enables this payload to be more easily deployed to the more remote missile ranges.

By its ability to function at high pressures, the wedge spectrometer demonstrated that it has a capability of making measurements in the D-region without the necessity of pumping through an orifice; thus, it measures with an open source region which may become important as more knowledge about the chemistry of this region is acquired. Difficulties have been observed with closed source regions in E-region measurements (von Zahn, 1967).

A major difficulty associated with the measurements in the D-region is estimating the influence of shock phenomena on the data that are obtained. The D-region is a region in which parachute technology has only been scantily developed; hence, supersonic speeds have been the rule in mass spectrometric measurements made to date. Sonin (1966) has theoretically treated the blunt nose configuration of Narcisi, and Burke and Miller (1968, 1969) have experimentally simulated with plasma jets the effects of this configuration moving through the ionosphere. Both papers have described problems associated with the protonated water clusters that have been observed by Narcisi (1967). Ferguson and Fehsenfeld (1969) have indicated that a sampling method that does not destroy these clusters is highly desirable. A possible advantage of the wedge spectrometer is that the source region may reside ahead or be partially free of the shock associate with the collector, sides, top, and bottom of the wedge structure. With an orifice arrangement, the source region always resides behind the shock. The sides, top, and bottom of the wedge have been perforated to permit easier flow. The grids of the spectrometer are 85 percent transparent and the possibility exists that shock effects may be negligible. Private communications were held with several aerodynamists but none would commit himself to a definite statement of the shocks associated with the grids. Perhaps, it would prove to be interesting studying the gas dynamic effects of these grids.

The ability to function at high pressures has been bought with a loss in resolving power. The resolving power of the instrument in the laboratory is considerably dependent on the source. The ionosphere should provide ions with a thermal energy spread thus the resolving power of the instrument will be higher. It is hoped that the data acquired will be of sufficient quality so as to be able to apply deconvolution methods. These methods enable the unfolding of overlapped peaks. Some computers methods have been described by Kendall (1961, 1962, 1967), Zabielski (1966), Rarick (1970). Enhancements in effective resolving power up to a factor of 8 have been made which would provide a resolving power of at least 40 for this instrument.

In order to obtain the maximum amount of information from a given flight of this payload, a total ion concentration measurement should be flown at the same time. It is not possible to place this additional measuring device on the present payload. However, Hale (1967) has developed a payload for small vehicles that could be launched nearly simultaneously with this mass spectrometer experiment. When the payload is modified for flight on a large vehicle, total ion concentration experiments should be incorporated into the payload. A blunt probe (Hale, 1967) mounted beside a spectrometer and a Langmuir probe mounted on an arm extending from the side of the vehicle would allow a positive and a negative ion spectrometer to be flown side by side.

The payload has been developed primarily for the D-region. However, it can also have immediate application in the upper F-region where the primary ions are H^+, He^+, and O^+. By laboratory measurements, it has more than adequate resolving power and it has the desirable open source region.

Bibliography

Biondi, M.A., Symp. on Lab. Meas. of Aeronomic Interest, York Univ., Toronto, Canada, 2 (1968).

Bourdeau, R.E., A.C. Aikin and J.L. Donley, J. Geophy. Res. 71, 727 (1966).

Boyd, R.L.F., and D. Morris, Proc. Phys. Soc. (London) 68, 1 (1955).

Boyd, R.L.F., Proc. Phys. Soc. (London) Ser. A. 253, 513 (1959).

Boyd, R.L.F., Nature 186, 749 (1960).

Burke, R.R., and W.J. Miller, Proc. of Seventeenth Annual Conf. on Mass Spectrometry and Allied Topics, Dallas, Texas, 257 (1969).

Cameron, A.E., and D.F. Eggers, Jr., Rev. Sci. Instr. 19, 605 (1948).

Chapman, S., Proc. Phys. Soc. (London) 43, 26 (1931).

Cuffin, B.N., Ionosphere Res. Lab., The Pennsylvania State Univ., Sci. Rpt. No. 249 (1965).

Datz, S. and E. Taylor, J. Chem. Phys. 25, 389 (1956).

Diem, H.T., Ionosphere Res. Lab., The Pennsylvania State Univ., Sci. Rpt. No. 309 (1967).

Donahue, T.M., (private communication) 1968).

Ferguson, E.E., and F.C. Fehsenfeld, J. Geophys. Res. 74, 5743 (1969).

Glenn, W.E., UCRL-1511, October, 1951.

Glenn, W.E., AECD-3337 (UCRL-1628), January, 1952.

Hale, L.C., Ionosphere Res. Lab., The Pennsylvania State Univ., Final Rpt. ARO-D Project No. 4515-E (1967).

Hasted, J.B., Physics of Atomic Collisions, Butterworths, Washington, D.C. 1964.

Hedin, A.E., and A.O. Nier, J. Geophys. Res. 70, 1273 (1967).

Hoffman, J.H., Science 155, 322 (1967).

Hoffman, J.H., Proc. IEEE 57, 1063 (1969)

Holmes, J.C. and C.Y. Johnson, Astronautics 4, 30 (1959).

Istomin, V.G., Geomagnetizm i Aeronomiya 3, 359 (1961).

Istomin, V.G., Space Research 3, 209 (1963).

Johnson, C.Y. and E.B. Meadows, J. Geophys. Res. 60, 193 (1955).

Johnson, C.Y. and J.P. Heppner, J. Geophys. Res. 60, 533 (1955).

Katzenstein, H.S. and S.S. Friedland, Rev. Sci. Instr. 26, 324 (1955).

Keller, R., Helv. Phys. Acta. 22, 386 (1949).

Kendall, B.R.F., Rev. Sci. Instr. 32, 758 (161).

Kendall, B.R.F., Rev. Sci. Instr. 33, 30 (1962).

Kendall, B.R.F., and H.M. Luther, Amer. J. Phys. 34, 580 (1966).

Kendall, B.R.F., and M.F. Zabielski, Proc. of Fifteenth Annual Conf. on Mass Spectrometry and Allied Topics, Denver, Colorado, 377 (1967).

MacKenzie, E.C., "The Investigation of Ionospheric Electron Density and Ion Composition Using Rocket-Borne Probes", Electron Phys. Dept., Univ. of Birmingham, London, Ph.D. Thesis, 1964.

Narcisi, R.S. J. Geophys. Res. 70, 3685 (1965).

Narcisi, R.S., Ann. Geophys. 22, 224 (1966).

Narcisi, R.S., Space Research 7, 186 (1967).

Narcisi, R.S., A.D. Bailey, and L. DellaLucca, Space Research 7, 446 (1967).

Narcisi, R.S., (private communication) 1968.

Narcisi, R.S., (private communication) 1969.

Paul, W. and M. Raether, Z. Physik 140, 262 (1955).

Pokhunkov, A.A., Space Research 1, 101 (1960).

Pokhunkov, A.A., Space Research 3, 132 (1963).

Rarick, J.P., Ionosphere Res. Lab., The Pennsylvania State Univ., Sci. Rpt. (to be published).

Sayers, J., Proc. Roy. Soc. (London), Ser. A. 253, 522 (1959).

Schaeffer, E.J., and M. Nichols, J. Geophys. Res. 69, 4649 (1964).

Sonin, A., J. Geophys. Res. 72, 4547 (1967).

Stephens, W.E., Phys. Rev. 69, 691 (1946).

Takekoshi, H., K. Tsurocka, and S. Shimizer, Bull. Inst. Chem. Res., Kyoto Univ. 27, 52 (1951).

Townsend, J.W., Rev. Sci. Instr. 23, 538 (1952).

von Zahn, U., J. Geophys. Res. 72, 5933 (1967).

Wiley, W.C., and I.H. McLaren, Rev. Sci. Instr. 26, 1150 (1955).

Willis, R.G., Ionosphere Res. Lab., The Pennsylvania State Univ., Sci. Rpt. No. 245 (1965).

Wolff, M.M., and W.E. Stephens, Rev. Sci. Instr. 24, 616 (1953).

Zabielski, M.F., Ionosphere Res. Lab., The Pennsylvania State Univ., Sci. Rpt. No. 280 (1966).

Zabielski, M.F., H.T. Diem, and B.R.F. Kendall, Proc. of Sixteenth Annual Conf. on Mass Spectrometry and Allied Topics, Pittsburgh, Pennsylvania, 202 (1968)

Zahringer, J., (presented at but deleted from), Proc. of Seventeenth Annual Conf. on Mass Spectrometry and Allied Topics, Dallas, Texas, (1969).